TITLE: Organelle proteomic profiling reveals lysosomal heterogeneity in association with longevity

AUTHOR: Yong Yu[1,2,#,*], Shihong M. Gao[3,4,#], Youchen Guan[4,5,#], Pei-Wen Hu[2], Qinghao Zhang[2], Jiaming Liu[1], Bentian Jing[1], Qian Zhao[2], David M Sabatini, Monther Abu-Remaileh[6,8], Sung Yun Jung[7], Meng C. Wang[2,4,*]

1. Current address: State Key Laboratory of Cellular Stress Biology, School of Life Sciences, Faculty of Medicine and Life Sciences, Xiamen University, Xiamen 361102, China

2. Huffington Center on Aging, Baylor College of Medicine, Houston TX, USA 77030

3. Developmental Biology Graduate Program, Baylor College of Medicine, Houston TX, USA 77030

4. Janelia Research Campus, Howard Hughes Medical Institute, Ashburn VA, USA 20147

5. Molecular and Cellular Biology Graduate Program, Baylor College of Medicine, Houston TX, USA 77030

6. Department of Chemical Engineering and Genetics, Stanford University, Stanford CA, USA 94305

7. Department of Molecular and Cellular Biology, Baylor College of Medicine, Houston TX, USA 77030

8. Institute for Chemistry, Engineering and Medicine for Human Health (ChEM-H), Stanford University, Stanford, CA 94305, USA

# Equal contribution

* Correspondence and requests for materials should be addressed to Meng C. Wang (mengwang@janelia.hhmi.org) or Yong Yu (yuy@xmu.edu.cn)

ABSTRACT

Lysosomes are active sites to integrate cellular metabolism and signal transduction. A collection of proteins associated with the lysosome mediate these metabolic and signaling functions. Both lysosomal metabolism and lysosomal signaling have been linked to longevity regulation; however, how lysosomes adjust their protein composition to accommodate this regulation remains unclear. Using deep proteomic profiling, we systemically profiled lysosome-associated proteins linked with different longevity mechanisms. We further discovered the lysosomal recruitment of AMPK and nucleoporin proteins and their requirements for longevity in response to increased lysosomal lipolysis. Through comparative proteomic analyses of lysosomes from different tissues and labeled with different markers, we discovered lysosomal heterogeneity across tissues as well as the specific enrichment of the Ragulator complex on Cystinosin positive lysosomes. Together, this work uncovers lysosomal proteome heterogeneity at different levels and provides resources for understanding the contribution of lysosomal protein dynamics to signal transduction, organelle crosstalk and organism longevity.

INTRODUCTION

Lysosomes are membrane-bound organelles that are specialized to constitute an acidic environment in the cytosol. Lysosomes carry many of proteins that are essential for maintaining lysosomal activities and mediating lysosomal regulatory effects. Inside the lysosomal lumen, a

47 series of acidic hydrolases, including lipases, proteases, glucosidase, acid phosphatase, nuclease
48 and sulfatases, are responsible for the degradation and recycling of extracellular and intracellular
49 materials delivered through endocytic, phagocytotic and autophagic processes (Appelqvist et al.,
50 2013; Ballabio & Bonifacino, 2020; Lawrence & Zoncu, 2019). Additionally, on the lysosomal
51 limiting membrane, a group of integral transmembrane proteins play crucial roles in the
52 maintenance of luminal acidic pH and ion homeostasis, the control of lysosomal membrane
53 potential and export of metabolic products, as well as the regulation of organelle interaction and
54 signal transduction (Ballabio & Bonifacino, 2020; Lawrence & Zoncu, 2019). For example, the
55 lysosomal vacuolar-type H^+-ATPase (v-ATPase) on the membrane is the primary driver for the
56 active accumulation of protons in the lysosomal lumen, which also requires a neutralizing ion
57 movement mediated by ion channels and transporters (Graves et al., 2008; Nicoli et al., 2019). In
58 addition, v-ATPase coordinates with lysosomal amino acid transporter SLC38A9 and lysosomal
59 cholesterol exporter NPC1 in regulating the activation of mechanistic/mammalian target of
60 rapamycin complex I (mTORC1) by amino acid and lipid cues (Castellano et al., 2017; Wang et
61 al., 2015). The recruitment of mTORC1 to the lysosome is mediated by RagA/B and RagC/D
62 GTPase heterodimers that are associated with the scaffold protein complex Ragulator tethered on
63 the lysosomal membrane (de Araujo et al., 2017). Through interacting with Axin, Ragulator also
64 mediates the activation of AMP-activated protein kinase (AMPK) on the lysosomal surface
65 (Zhang et al., 2014). Furthermore, lysosomes are not static, isolated organelles; instead they are
66 highly mobile vesicles that undergo frequent movements in both anterograde (nucleus-to-
67 periphery) and retrograde (periphery-to-nucleus) directions and form dynamic interactions with
68 other organelles including endosomes, autophagosomes, endoplasmic reticulum and
69 mitochondria (Ballabio & Bonifacino, 2020; Pu et al., 2016). These trafficking and interaction

70 processes are mediated by lysosomal integral transmembrane proteins as well as diverse proteins
71 that are recruited to lysosomes in response to different extracellular and intracellular inputs
72 (Ballabio & Bonifacino, 2020; Pu et al., 2016).
73
74 Lysosomes control numerous cellular processes, and dysfunction of lysosomes has been linked
75 with various diseases, such as lysosomal storage disorders (Ballabio & Gieselmann, 2009; Platt
76 et al., 2012), Alzheimer's disease (Nixon & Cataldo, 2006), Parkinson disease (Navarro-Romero
77 et al., 2020) and some types of cancer (Davidson & Vander Heiden, 2017; Fehrenbacher &
78 Jaattela, 2005). Emerging evidence also suggests the lysosome as a central regulator of organism
79 longevity, through its involvement in autophagy and its modulation of metabolic signaling
80 pathways. The induction of autophagic flux has been observed in multiple pro-longevity states,
81 and is required for the pro-longevity effects caused by those genetic, dietary and
82 pharmacological interventions, such as reduced insulin/IGF-1 signaling, caloric restriction and
83 spermidine treatment (Hansen et al., 2018). On the other hand, lysosomes are now recognized as
84 the key platform to modulate the activities of mTORC1 and AMPK signaling, two well-
85 characterized longevity regulating pathways (Savini et al., 2019). In addition, our studies have
86 discovered lysosomal lipid messenger pathways that are induced by a lysosomal acid lipase
87 LIPL-4 and promote longevity via both cell-autonomous and cell-nonautonomous signaling
88 mechanisms (Folick et al., 2015; Ramachandran et al., 2019; Savini et al., 2022; Wang et al.,
89 2008). Given the importance of lysosomes in regulating longevity, it will be crucial to
90 understand how changes in the lysosomal protein composition are associated with longevity
91 regulation.
92

93 To systemically profile the protein composition of lysosomes, methods have been developed to
94 purify lysosomes using gradient centrifugation (Gao et al., 2017; Lubke et al., 2009; Markmann
95 et al., 2017; Schroder et al., 2010). More recently, a lysosome immunoprecipitation method,
96 which uses anti-HA (human influenza virus hemagglutinin) antibody conjugated magnetic beads
97 to immune-purify lysosomes from mammalian cells expressing transmembrane protein 192
98 (TMEM192) fused with three tandem HA (3×HA) epitopes, has further improved the specificity
99 and speed of lysosomal isolation (Abu-Remaileh et al., 2017). This rapid isolation method has
100 facilitated follow-up mass spectrometry (MS)-based proteomics as well as metabolomics
101 analyses (Abu-Remaileh et al., 2017; Eapen et al., 2021; Laqtom et al., 2022).
102
103 In the present study, we have applied an immunoprecipitation-based method for rapid isolation
104 of lysosomes from live *C. elegans* using transgenic strains expressing lysosomal membrane
105 proteins tagged with 3×HA (Lyso-Tag). We then conducted large-scale proteomic profiling using
106 isolated lysosomes and remaining non-lysosomal fractions, to determine the enrichment of each
107 identified protein on the lysosome. Based on these analyses, we have defined a lysosome-
108 enriched proteome and compared it between wild-type and long-lived worms, revealing
109 lysosomal protein composition changes associated with longevity. We have also generated
110 transgenic strains expressing Lyso-Tag specifically in the hypodermis (epidermal), muscle,
111 intestine (fat storage/digestion) and neurons, leading to the discovery of lysosomal proteome
112 heterogeneity in different tissues. Furthermore, by comparing the lysosome-enriched proteome
113 with LAMP1/LMP-1 Lyso-Tag and the one with Cystinosin/CTNS-1 Lyso-Tag, we discovered
114 that the Ragulator complex and other mTORC1 regulators exhibit increased enrichments on
115 lysosomes containing the cysteine transporter Cystinosin.

116

117 **RESULTS**

118

119 **Map lysosome-enriched proteome systemically in *C. elegans***

120

121 To comprehensively reveal proteins that are enriched at the lysosome, we have applied rapid
122 lysosome immunoprecipitation followed by MS-based proteomic profiling (Lyso-IP) (Figure
123 1A). We first generated a transgenic strain expressing the lysosome-associated membrane
124 protein, LMP-1 (Eskelinen, 2006) fused to both 3×HA and RFP (LMP-1 *LysoTg*). Fluorescence
125 imaging of RFP confirmed the lysosomal localization of the LMP-1 fusion protein in live
126 organisms and made it possible to follow purified lysosomes *in vitro* (Figure 1B). The 3×HA
127 epitope tag is used to purify lysosomes from homogenized worm lysate via immunoprecipitation
128 using anti-HA antibody conjugated magnetic beads (Figure 1A). In general, about 160,000
129 worms at day-1 adulthood were harvested and homogenized. Upon centrifugation to remove
130 debris and nuclei, 3×HA-tagged lysosomes were immunoprecipitated and separated from other
131 cellular content (flow-through controls, Figure 1A). The whole process from harvesting worms
132 to purified lysosomes takes around 25 minutes. Many purified lysosomes were able to take up
133 LysoTracker probes and exhibit positive fluorescence signals, indicating that they maintain intact
134 with an acidic pH; while there are also some broken lysosomes losing LysoTracker staining
135 (Figure 1C). When blotting with antibodies against different organelle markers, we found that
136 the purified lysosomes show no or nearly no protein markers of other organelles, including HSP-
137 60 (mitochondria heat shock protein) (Hartl et al., 1992; Mayer, 2010), CYP-33E1 (Endoplasmic
138 Reticulum (ER) cytochrome P450) (Brown & Black, 1989), SQV-8 (Golgi

139 glucuronosyltransferase) (Hadwiger et al., 2010) and beta-actin (cytoskeleton) (Figure 1D),
140 while the flow-through controls show these protein markers but nearly no lysosomal protein
141 marker LMP-1 (Figure 1D). Together, these results demonstrate the efficacy of the Lyso-IP
142 approach to enrich for lysosomal proteins.
143
144 Next, we conducted proteomic profiling of purified lysosomes with their paired flow-through
145 controls (Figure 1A). The correlation analysis shows good reproducibility among four
146 independent biological replicates (Supplementary Figure 1A), and the PCA analysis shows a
147 clear separation between Lyso-IP replicates and flow-through controls (Figure 1E). In parallel,
148 we also conducted immunoprecipitation using homogenized lysate from wild-type (WT) worms
149 that do not carry a Lyso-Tag and then analyzed proteomic profiles of three independent samples
150 as non-tag controls (Figure 1A). Based on these proteomic data, we used three criteria to identify
151 lysosome-enriched proteins: first, their levels in the purified lysosomes are 10-fold or higher than
152 those in the flow-through controls (Figure 2A); second, their enrichments can be repeated in all
153 biological replicates (Figure 2A); and lastly, their enrichments over non-tag controls are more
154 than 2-fold (Figure 2B).
155
156 Together, 216 lysosome-enriched candidates were identified from more than 6000 detected
157 proteins, and 178 candidates have mammalian homologs (Supplementary Figure 1B,
158 Supplementary Table 1). This lysosome-enriched proteome consists of 83 membrane transporters
159 and channels, 47 enzymes, 26 signaling factors, 12 structural components, and 6 involved in
160 vesicle trafficking (Figure 2C). These include known lysosomal proteins, such as various
161 lysosomal Cathepsins that catalyze protein degradation (Turk et al., 2012), lysosomal specific

162 ARL8 GTPase that mediates lysosome trafficking (Nakae et al., 2010), and subunits of
163 lysosomal v-ATPase that pumps protons into the lysosomal lumen to maintain an acidic pH
164 (Forgac, 2007) (Supplementary Table 1).
165
166 Lysosomal v-ATPase consists of both V0 and V1 domains that are associated with the lysosomal
167 membrane and faced the cytosol, respectively. Reversible dissociation of the V1 and V0 domains
168 responds to nutritional signals and plays a crucial role in the regulation of the lysosomal v-
169 ATPase activity (Kane, 1995; McGuire & Forgac, 2018; Ratto et al., 2022; Stransky & Forgac,
170 2015). Except for VHA-18 (V1 H subunit), we were able to detect all other subunits of
171 lysosomal v-ATPase, including VHA-5, 6, 7 and UNC-32 (V0 a subunits), VHA-1, 2, 3 and 4
172 (V0 c subunits), VHA-16 (V0 d subunit), VHA-17 (V0 e subunit), VHA-13 (V1 A subunit),
173 VHA-12 (V1 B subunit), VHA-11 (V1 C subunit), VHA-14 (V1 D subunit), VHA-8 (V1 E
174 subunit), VHA-9 (V1 F subunit), VHA-10 (V1 G subunit), and VHA-15 (V1 H subunit), and
175 also two v-ATPase transporting accessory proteins, VHA-19 and VHA-20 (Figure 2D,
176 Supplementary Table 1). Among the V0 domain subunits, VHA-4, 5, 6, 7 and 16 and UNC-32
177 are enriched over 10-fold in all four replicates, VHA-1, 2 and 3 are enriched over 10-fold in
178 three replicates and over 5-fold in one replicate, and the low abundant VHA-17 was only
179 detected in two replicates, with more than 10-fold enrichments in both (Figure 2D). The VHA-19
180 transporting accessory protein is enriched over 10-fold in two replicates and less than 5-fold in
181 two replicates (Figure 2D). In contrast, for the subunits of the V1 domain and the VHA-20
182 transporting accessory protein, they show no enrichment in the purified lysosomes compared to
183 the flow-through controls (Figure 2D). These results suggest that the free form of the V1 domain

184 and the associated form bound with the V0 domain at lysosomes both exist under the well-fed
185 condition in wild-type worms.
186
187 In addition to 30.7% of proteins with known lysosome/endosome localization, the lysosome-
188 enriched proteome includes a small portion of proteins localized to other cellular organelles,
189 ER/Golgi (6.0%), mitochondria (1.4%), peroxisome (0.4%), lipid droplet (0.9%), and synaptic
190 vesicle (1.8%) (Figure 2E). On the other hand, there is a large portion of proteins with annotated
191 plasma membrane localization (24.8%) (Figure 2E). Many of these plasma membrane proteins
192 are receptors that are known to be subject to endocytosis and subsequent recycling lysosomal
193 degradation, such as INA-1/integrin alpha-6 (De Franceschi et al., 2015), VER-3/vascular
194 endothelial growth factor receptor (Ewan et al., 2006), PTC-1/protein patched receptor (Gallet &
195 Therond, 2005), and IGLR-2/leucine-rich repeat-containing G-protein coupled receptor (Snyder
196 et al., 2013) (Supplementary Table 1) (Braulke & Bonifacino, 2009). We also identified proteins
197 involved in the endocytosis process, including low-density lipoprotein receptor-related proteins,
198 LRP-1 (Grant & Hirsh, 1999) and arrestin domain-containing proteins, ARRD-13 and ARRD-18
199 (Kang et al., 2014) (Supplementary Table 1) that mediate the internalization of plasma
200 membrane receptors (Ma et al., 2002). Thus, the lysosome-enriched proteome also reveals
201 membrane receptor proteins that undergo recycling through the endo-lysosomal system.
202
203 **Lysosome-enriched proteome alterations associate with longevity**
204
205 Lysosomes are known as a heterogeneous population of vesicles, differing in their size, shape,
206 pH and cellular distribution. Considering the emerging role of lysosomes as a cellular hub to

207 integrate protein signals and regulate longevity, we expect that the protein composition of
208 lysosomes may exhibit heterogeneity in association with different longevity mechanisms. To test
209 this hypothesis, we crossed LMP-1 *LysoTg* with the long-lived *lipl-4* transgenic strain (*lipl-4 Tg*)
210 that constitutively expresses a lysosomal acid lipase (Wang et al., 2008) and also the long-lived
211 loss-of-function mutant of *daf-2* (*daf-2(lf)*) that encodes the insulin/IGF-1 receptor (Kenyon et
212 al., 1993; Martins et al., 2016). Reducing insulin/IGF-1 signaling is a well-conserved mechanism
213 to promote longevity in diverse organisms ranging from *C. elegans, Drosophila,* mice to humans
214 (Kenyon et al., 1993; Martins et al., 2016). We conducted Lyso-IP proteomic analyses and
215 compared lysosome-enriched proteomes between wild-type and long-lived strains. The
216 correlation analysis shows good reproducibility among three independent biological replicates
217 (Supplementary Figure 1C, 1D), and the PCA analysis shows a clear separation between Lyso-IP
218 replicates and flow-through controls (Supplementary Figure 1E).
219
220 Using LMP-1 Lyso-IP, we have identified 449 lysosome-enriched proteins in the *lipl-4 Tg*
221 worms (Supplementary Table 2), and 176 of them overlap with the LMP-1 Lyso-IP candidates
222 from WT worms (Figure 3A). Thus, 82% of proteins enriched on WT lysosomes are also
223 enriched on *lipl-4 Tg* lysosomes; however, 61% of proteins enriched on *lipl-4 Tg* lysosomes are
224 absent in WT lysosomes (Figure 3A). Interestingly, among the proteins that are specific to *lipl-4*
225 *Tg* lysosomes, there are autophagosome proteins and proteins that mediate the fusion between
226 autophagosomes and lysosomes, including ATG-9/ATG9A(Popovic & Dikic, 2014), EPG-
227 7/RB1CC1 (Nishimura et al., 2013), VAMP-7/VAMP8 (Diao et al., 2015; Itakura et al., 2012)
228 and Y75B8A.24/PI4KIIα (Sugiura et al., 1989) (Figure 3B), suggesting that autophagy is

229 induced by *lipl-4 Tg*. Consistently, the induction of autophagy has been reported in the *lipl-4 Tg*
230 worms, which is required for the longevity effect (Lapierre et al., 2011).
231
232 In addition, we found that the Ragulator complex, LMTR-2/LAMTOR2, LMTR-3/LAMTOR3
233 and LMTR-5/LAMTOR5, that serves as a scaffold for the activation of mTORC1 and AMPK
234 (Zhang et al., 2014) is more specifically enriched at the lysosome from the *lipl-4 Tg* worms than
235 WT (Figure 3B). There are two homologs of AMPK catalytic units, AAK-1 and AAK-2 in *C.*
236 *elegans.* We found that AAK-2 is enriched more than 10-fold in the Lyso-IP samples compared
237 to the flow-through controls from the *lipl-4 Tg* worms, but it is only detected in the flow-through
238 controls from WT worms (Figure 3C). Likely due to its low abundance, AAK-1 was detected
239 twice in the Lyso-IP samples from the *lipl-4 Tg* worms but once only in the flow-through sample
240 from WT worms (Figure 3C). These results suggest that AMPK is specifically recruited to the
241 lysosomal surface and becomes activated to promote longevity in the *lipl-4 Tg* worms. In
242 supporting this idea, we found that the inactivation of AMPK using the *aak-2* loss-of-function
243 mutant together with the *aak-1* RNA interference (RNAi) knockdown reduces the lifespan
244 extension in the *lipl-4 Tg* worms from 72% to 40% (Figure 3D, Supplementary Table 3). Thus,
245 the lysosomal activation of AMPK responds to LIPL-4-induced lysosomal lipolysis and mediates
246 the longevity regulation.
247
248 Moreover, compared to WT lysosomes, the enrichment of lysosomal v-ATPase is higher in *lipl-4*
249 *Tg* lysosomes, especially for the V0 subunits, VHA-1, 2, 3 the V1 subunits, VHA-11 and VHA-
250 15, and the v-ATPase transporting accessory proteins, VHA-19 and VHA-20 (Figure 3B). There
251 are also 13 lysosomal channels/transporters, including T14B4.3/ATP6AP2, the proton-

252 translocating ATPases required for the v-ATPase-mediated lysosomal acidification (Cruciat et
253 al., 2010) and CLH-6/CLCN7, the H(+)/Cl(-) exchange transporter mediating the acidification of
254 the lysosome (Graves et al., 2008; Nicoli et al., 2019), and 16 lysosomal hydrolases that are
255 specifically associated with the *lipl-4 Tg* lysosomes (Figure 3B). Together, these results suggest
256 that the proportion of mature lysosomes is increased in the *lipl-4 Tg* worms, which may lead to
257 increased autophagy, the lysosomal activation of AMPK, and consequently the induction of
258 longevity.
259
260 In parallel, 259 lysosome-enriched proteins were identified in the *daf-2(lf)* mutant using LMP-1
261 Lyso-IP (Supplementary Table 4), 147 of them overlapping with the LMP-1 Lyso-IP candidates
262 from WT worms, 197 of them overlapping with the LMP-1 Lyso-IP candidates from the *lipl-4*
263 *Tg* worms, and 55 unique to the *daf-2(lf)* mutant (Figure 3A). The *daf-2(lf)* lysosome-enriched
264 proteome shows enrichment of autophagic components, including ATG-9/ATG9A (also shown
265 in *lipl-4 Tg* lysosome-enriched proteome) and the autophagy receptor SQST-1/SQSTM1 (Figure
266 3B), which supports the previously reported induction of autophagy in the *daf-2(lf)* mutant. On
267 the other hand, the Ragulator complex components LMTR-2/3/5 were not more enriched in the
268 lysosome from the *daf-2(lf)* mutant than that from WT worms (Figure 3B). For the AMPK
269 catalytic subunits, AAK-2 was not identified in the lysosome-enriched proteome from the *daf-*
270 *2(lf)* mutant, and the low abundant AAK-1 was not detected in either Lyso-IP or flow-through
271 samples (Figure 3C). It is known that the activation of AMPK displays high spatial specificity in
272 the cell when responding to different upstream stimuli (Khan & Frigo, 2017). In *C. elegans,* it
273 was previously shown that AAK-2 mediates the longevity effect conferred by the *daf-2(lf)*
274 mutant (Apfeld et al., 2004). Our results indicate that this regulation might not be associated with

275 the lysosomal activation of AMPK. Thus, the spatial specificity of AMPK activation at different
276 subcellular compartments may be linked with different longevity mechanisms.
277
278 **Enhanced lysosome-nucleus interaction mediates longevity**
279
280 In our previous studies, we found that upon LIPL-4-induced lysosomal lipolysis, a lysosome-to-
281 nucleus retrograde lipid messenger signaling pathway is activated in intestinal cells to promote
282 longevity (Folick et al., 2015; Ramachandran et al., 2019; Savini et al., 2022; Wang et al., 2008).
283 Interestingly, when analyzing the LMP-1 lysosome-enriched proteome in the *lipl-4 Tg* worms,
284 we found an enrichment of nucleus-localized proteins (Figure 4A), including two nucleoporin
285 proteins NPP-6/Nup160 and NPP-15/Nup133 in the Nup160 complex that localizes at the basket
286 side of the nuclear pore (Figure 4B) (Vasu et al., 2001). Such enrichment of nucleoporin proteins
287 was not found in the LMP-1 lysosome-enriched proteome of either WT or the *daf-2(lf)* mutant
288 (Figure 4B). In the cell, mobile lysosomes change their distribution along the perinuclear-
289 peripheral axis in response to different nutrient signals and metabolic status (Ballabio &
290 Bonifacino, 2020; Pu et al., 2016). Moreover, it is known that the cellular position of lysosomes
291 affects their luminal pH, with perinuclear lysosomes being more acidic (Johnson et al., 2016).
292 We found that the lysosome-enriched proteome of the *lipl-4 Tg* worms consists of lysosomal v-
293 ATPase V1 subunits, proton-translocating ATPase and exchanging ion transporters that mediate
294 lysosomal acidification, but these components were not enriched in the WT lysosome proteome
295 (Figure 3B), supporting that lysosomes are more acidic in the *lipl-4 Tg* worms. We thus
296 hypothesize that LIPL-4-induced lysosomal lipolysis may enhance the interaction between

297 lysosomes and the nucleus and further facilitate the lysosome-to-nucleus retrograde lipid
298 signaling to promote longevity.
299
300 To test this hypothesis, we imaged lysosomal positions in intestinal cells where *lipl-4* is
301 expressed. Using a dual reporter strain expressing both lysosomal LMP-1::RFP fusion and
302 nucleus-localized GFP, we found that lysosomes exhibit a dispersed pattern in the intestinal cell
303 of WT worms (Figure 4D). However, in the *lipl-4 Tg* worms, lysosomes are clustered in the
304 perinuclear region (Figure 4D), supporting the hypothesis that the lysosome-nucleus interaction
305 is enhanced. To quantitatively measure this change in lysosomal positioning, we analyzed the
306 RFP fluorescent signal distribution in intestinal cells (Supplementary Figure 2A). We found the
307 perinuclear and peripheral distribution of lysosomes in the *lipl-4 Tg* worms is significantly
308 increased and decreased, respectively, compared to WT worms ($p<0.01$, Figure 4C, 4D,
309 Supplementary Figure 2B). In contrast, such perinuclear clustering is not observed in intestinal
310 cells of the *daf-2(lf)* mutant (Figure 4E, 4F, Supplementary Figure 2C). Moreover, we found that
311 the RNAi knockdown of *npp-6* suppresses the lifespan extension in the *lipl-4 Tg* worms (Figure
312 4G, 4H) but does not affect the lifespan extension in the *daf-2(lf)* mutant (Figure 4I, 4J). These
313 results suggest that the enhanced lysosome-nucleus interaction is specifically related to LIPL-4-
314 induced lysosomal signaling and longevity.
315
316 Together, these studies discover changes in the lysosome-enriched proteome between WT and
317 different long-lived strains and reveal that the lysosomal proteome composition can be
318 influenced by the metabolic status of the lysosome and its interaction with other organelles and
319 in turn correlates with lysosomal signaling and longevity regulation.

320

321 **Profile lysosome-enriched proteome heterogeneity among different tissues**

322

323 Tissue-specific regulation of longevity has been reported in various organisms. To examine how
324 lysosome-enriched proteomes exhibit heterogeneity among different tissues, we have generated
325 four transgenic strains that express LMP-1 Lyso-Tag specifically in neurons, muscle, intestine
326 and hypodermis using tissue-specific promoters, *unc-119*, *myo-3*, *ges-1* and *col-12*, respectively
327 (Figure 5A). Using these transgenic strains, we purified lysosomes in a tissue-specific manner
328 and conducted proteomic profiling. The correlation analysis shows good reproducibility among
329 three independent biological replicates (Supplementary Figure 3A-D).

330

331 Unlike the whole-body Lyso-IP, the flow-through samples from tissue-specific Lyso-IP contain
332 not only non-lysosomal fractions from the targeted tissue but also lysosomes from non-targeted
333 tissues. Thus, these flow-through samples cannot be simply used as controls to determine the
334 enrichment of proteins at the lysosome in the targeted tissue. To assess tissue-specific changes,
335 we have normalized the level of each identified protein to the level of LMP-1 in the same
336 replicate, and then compared the normalized ratio between the whole-body Lyso-IP and the
337 tissue-specific Lyso-IP (Figure 5B-E, Supplementary Table S5). We found that among the 216
338 proteins identified from the whole-body Lyso-IP, 85 of them show comparable ratios between
339 the whole-body Lyso-IP and the four tissue-specific Lyso-IPs (Figure 5F, Group I), suggesting
340 relative homogenous lysosomal enrichments of these proteins among different tissues. Nine of
341 them were completely absent in the tissue-specific Lyso-IP, which may be related to their low
342 abundance (Figure 5F, Group IV). There are also proteins that were not detected in one or two

343 tissues but exhibited similar enrichments as the whole body Lyso-IP in other tissues, such as
344 PGP-6, an ABC transporter missing in the muscle-specific Lyso-IP, PBO-1, calcium-binding
345 protein P22 missing in the hypodermis-specific Lyso-IP and Y57G11C.33, Golgin A7 missing in
346 both the hypodermis- and neuron-specific Lyso-IPs, which may be associated with their lack of
347 expression and/or lack of lysosome enrichments in specific tissues.
348
349 Importantly, there are 122 proteins that exhibited significant difference in their enrichments
350 between the whole-body Lyso-IP and the tissue-specific Lyso-IPs ($p<0.05$), 56 of them (Group
351 II) showing an increase in the tissue-specific Lyso-IPs while the other 66 (Group III) showing a
352 decrease (Figure 5F). Some of them were only enriched in one tissue but remained unchanged in
353 others, including 15 proteins with higher ratios only in the intestine, 3 only in the hypodermis
354 and 5 only in neurons. There are also five proteins that showed an increased enrichment in one
355 tissue, but a decreased enrichment in another tissue, including AQP-1, an Aquaporin channel
356 with a higher ratio in neurons but a lower one in the hypodermis, Y58A7A.1 a copper uptake
357 transporter with a higher ratio in the hypodermis but a lower one in the muscle, PBO-4, a
358 sodium/hydrogen exchanger with a higher ratio in the intestine but a lower one in the
359 hypodermis, and two innexin proteins that form gap junctions in invertebrate animals, INX-17
360 with a higher ratio in neurons but a lower ratio in the hypodermis and INX-15 with a higher ratio
361 in the intestine but lower ratios in the muscle and hypodermis (Figure 5F). For these candidates,
362 there is a clear tissue preference regarding their lysosomal enrichments. Thus, the lysosomal
363 proteome is not only affected by the genotype of the organism, but also exhibits heterogeneity
364 among different tissues within the organism, which may be related to the metabolic status in each
365 tissue and consequently contribute to specific activities and signaling effects of the tissue. Our

366 studies provided a list of candidates for further investigation of the tissue-specific regulation of
367 lysosomal metabolism and signaling.
368
369 **Cystinosin positive mature lysosomes enrich specific lysosomal proteins**
370
371 The analysis of the candidates specifically detected in the *lipl-4 Tg* worms suggest that the
372 proportion of mature lysosomes may affect the lysosomal protein composition. Although LMP-1
373 is a well-established lysosomal protein marker and highly abundant on the lysosomal surface, it
374 can be also detected in late endosomes and sometimes in early endocytic compartments. With the
375 hope to profile proteins enriched in mature lysosomes, we chose CTNS-1, the *C. elegans*
376 lysosomal cystine transporter Cystinosin that is a well-established marker of mature lysosomes
377 (Gahl et al., 1982; Jonas et al., 1982; Kalatzis et al., 2001), and generated a transgenic strain
378 expressing CTNS-1 tagged with both 3×HA and RFP (CTNS-1 *lysoTg*). Fluorescence imaging of
379 RFP confirmed the lysosomal localization of the CTNS-1 fusion protein in live organisms
380 (Figure 6A). Using this transgenic strain, we followed the same Lyso-IP and MS profiling
381 pipeline. The correlation analysis shows good reproducibility among three independent
382 biological replicates (Supplementary Figure 1G), and the PCA analysis indicates a clear
383 separation between Lyso-IP samples and flow-through controls (Supplementary Figure 1F).
384 Using the same selection criteria, we identified 293 candidates whose levels are enriched at least
385 10-fold in the purified lysosomes than those in the flow-through controls among all independent
386 biological replicates and show over 2-fold enrichment compared to the non-tag controls
387 (Supplementary Table 6). There are 95 lysosome-enriched proteins shared between the LMP-1
388 and the CTNS-1 Lyso-IP proteomic profiling datasets (Figure 6B, Supplementary Table 6), and

389 47 of these shared proteins are annotated with lysosomal localization (Supplementary Table 6).
390 We have also crossed the CTNS-1 *lysoTg* strain with the *lipl-4 Tg* strain and the *daf-2(lf)* mutant
391 and then conducted Lyso-IP proteomic profiling. However, the pull-down efficiency was very
392 low in these long-lived worms, which prevents us to identify proteins unique to CTNS-1 Lyso-IP
393 in those conditions.
394
395 In WT worms, the proportions of the identified proteins with different categories of subcellular
396 annotation are comparable between LMP-1 and CTNS-1 Lyso-IP conditions (Figure 6C, 2E),
397 and for proteins with lysosomal annotation, the proportion is 25% and 28% in LMP-1 and
398 CTNS-1 Lyso-IP, respectively (Figure 6D). However, among the 121 proteins only identified in
399 LMP-1 Lyso-IP, there are only 8 with lysosomal annotation (7%); while for the 198 proteins
400 only identified in CTNS-1 Lyso-IP, 35 are with lysosomal annotation and the proportion remains
401 as 18% (Figure 6D). Among the lysosomal proteins that are unique to CTNS-1 Lyso-IP, there are
402 autophagosome proteins and proteins that mediate the fusion between autophagosomes and
403 lysosomes, including ATG-9/ATG9A (Popovic & Dikic, 2014), C33A11.2/DRAM2 (Crighton et
404 al., 2006), EPG-7/RB1CC1 (Nishimura et al., 2013), and VAMP-7/VAMP8 (Diao et al., 2015;
405 Itakura et al., 2012) (Figure 6E). CTNS-1 Lyso-IP unique candidates also include the Ragulator
406 complex components LMTR-2/3/5, the lysosomal amino acid transporter F13H10.3/SLC38A9
407 and the lysosomal calcium channel CUP-5/TRPML1 that regulate mTORC1 signaling (Li et al.,
408 2016; Rebsamen et al., 2015; Wang et al., 2015; Wyant et al., 2017) (Figure 6E). These results
409 suggest that CTNS-1 Lyso-IP enriches lysosomes that are actively involved in autophagy and
410 transduce mTORC1 signaling.
411

412 Furthermore, when systemically examining 85 lysosome-related proteins that were previously
413 annotated in *C. elegans* based on sequence homology (Sun et al., 2020), we found that many
414 lysosomal hydrolases exhibit increased enrichments with CTNS-1 Lyso-IP, especially for those
415 cysteine proteases including CPR-6, LGMN-1, CPL-1, CPZ-1 and TAG-196 (Figure 6F). These
416 enrichments are consistent with that CTNS-1 is located at mature lysosomes as a cysteine
417 transporter (Gahl et al., 1982; Jonas et al., 1982; Kalatzis et al., 2001). The similar increased
418 enrichments of lysosomal hydrolases were also observed in the LMP-1 Lyso-IP candidates
419 identified from the *lipl-4 Tg* worms (Figure 6F), further supporting that the long-lived *lipl-4 Tg*
420 worms carry more acidic lysosomes. Together, we found that lysosome-enriched proteomes
421 identified from both LMP-1 and CTNS-1 Lyso-IP consist of well-characterized lysosomal
422 enzymes and integral membrane proteins as well as proteins that contribute to lysosomal
423 signaling, dynamics and contact with other cellular compartments. Besides many known
424 lysosomal proteins, various proteins that are not previously linked with lysosomes are now
425 identified through these systemic analyses.
426
427 **Lysosome-enriched proteins regulate different lysosomal activities**
428
429 To understand the role of these newly identified lysosome-enriched proteins in regulating
430 lysosomal functions, we have examined their effects on lysosomes using an RNAi screen based
431 on LysoSensor fluorescence intensity. We focused on 95 lysosome-enriched proteins shared
432 between LMP-1 and CTNS-1 Lyso-IPs and knocked down their coding genes by RNAi, and then
433 used LysoSensor probes to stain lysosomes. From screening these 95 candidates (Supplementary
434 Table 7), we have identified five genes whose inactivation cause changes in LysoSensor signal

435 intensity, and four of them have human homologs, including two lysosomal v-ATPase subunits,
436 UNC-32/ATP6V0A and VHA-5/ATP6V0A, the lysosomal amino acid transporter SLC-
437 36.2/SLC36A1 (SLC36A4), and a transmembrane protein R144.6/TMEM144 (Supplementary
438 Table 7, Supplementary Figure 5). We further examined their effects on the lysosomal number,
439 size and pH. We found that the RNAi knockdown of the two lysosomal v-ATPase subunits,
440 UNC-32 and VHA-5, lead to decreased lysosomal numbers (Figure 7F), but an increase in the
441 lysosomal size (Figure 7G). Using fluorescence lifetime microscopy, we also found that the
442 RNAi knockdown of R144.6 and UNC-32 increases and decreases lysosomal pH, respectively
443 (Figure 7H).
444
445 UNC-32, VHA-5 and SLC-36.2 are well-known lysosomal proteins, but the subcellular
446 localization of the R144.6 protein remains unknown. R144.6 is a predicted carbohydrate
447 transporter, and structural simulation using AlphaFold2 suggested it as a solute carrier family
448 (SLC) transporter (Figure 7I). To characterize its subcellular localization, we have generated a
449 CRISPR knock-in line in which the endogenous R144.6 protein is fused with the fluorescent
450 protein NeonGreen and then stained these worms with LysoTracker Red to mark lysosomes. In
451 the hypodermis, we found that NeonGreen and LysoTracker Red signals overlap, confirming the
452 lysosomal localization of this newly identified transmembrane protein from Lyso-IP (Figure 7J).
453 On the other hand, its expression was not detected in the muscle, and in the intestine, its
454 NeonGreen signals were not overlapped with LysoTracker Red, which is consistent with tissue-
455 specific Lyso-IP analyses. R144.6 were enriched in the hypodermis-specific Lyso-IP at a similar
456 level as in the whole-body Lyso-IP; however, it was not detected in the muscle- or intestine-
457 specific Lyso-IP (Supplementary Table 5). These results further support the enrichment

458 specificity of proteins at the lysosome in different tissues as well as the power of the Lyso-IP
459 proteomic profiling in discovering new lysosomal proteins with functional significance.
460
461 **DISCUSSION**
462
463 Our studies reveal the heterogeneity of lysosomal protein composition that is associated with
464 lysosomal status, tissue specificity, and organism longevity. Through systemic profiling of
465 lysosome-enriched proteins under different conditions, we confirmed the induction of lysosome-
466 related autophagy by different longevity-promoting pathways, unveiled increased cellular
467 interaction between lysosomes and the nucleus upon the induction of lysosomal lipolysis and its
468 contribution to longevity regulation, and underlined the importance of the spatial control of
469 AMPK activation in regulating longevity. Our studies provide not only methods for future
470 studies to profile the dynamics of the lysosomal proteome in response to diverse physiological
471 inputs, but also resources for understanding the vital contribution of these dynamics in
472 modulating signal transduction, organelle crosstalk and organism longevity.
473
474 These proteomic studies reveal changes in the interaction between lysosomes and other
475 organelles under different conditions. One example is the lysosome-nucleus interaction. In the
476 Lyso-IP fraction from WT worms, we did not detect any proteins with sole nuclear localization;
477 however, in the Lyso-IP fraction from the *lipl-4 Tg* or *daf-2(lf)* mutant worms, nuclear proteins
478 were identified and the percentage of the increase over WT is significantly higher in the *lipl-4 Tg*
479 worms ($p<0.05$, Figure 4A, Supplementary Figure 4). Based on this finding, we discovered the
480 previously unknown perinuclear accumulation of lysosomes in the *lipl-4 Tg* worms (Figure 4C,

481 4D) and further confirmed its importance for longevity regulation (Figure 4G, 4H). It is shown
482 previously that perinuclear lysosomes are more acidic than peripheral lysosomes (Johnson et al.,
483 2016; Webb et al., 2021). Thus, the increase in perinuclear lysosomes may be associated with the
484 increased proportion of mature lysosomes in the *lipl-4 Tg* worms, which is supported by the
485 increased enrichments of lysosomal v-ATPase, channels/transporters and hydrolases (Figure 3B).
486 This increased distribution of lysosomes toward the perinuclear region could facilitate proteins
487 and metabolites transporting from the lysosome to the nucleus through the nuclear pore and in
488 turn their signaling effects. On the other hand, we did not detect perinuclear accumulation of
489 lysosomes in the *daf-2(lf)* mutant worms by cellular imaging, and the nuclear proteins detected
490 through LMP-1 Lyso-IP from the *daf-2(lf)* mutant worms are mainly involved in RNA splicing.
491 In yeast cells, defects in pre-RNA processing have been associated with nucleophagy (Leger-
492 Silvestre et al., 2005) that involves SQSTM1 and lysosomes (Ivanov et al., 2013; Mijaljica &
493 Devenish, 2013). We thus speculate that the increased enrichment of nuclear proteins in the *daf-*
494 *2(lf)* mutant worms may be associated with the induction of nucleophagy but not changes in
495 lysosomal positioning.
496
497 mTORC1 and AMPK are key metabolic checkpoints that regulate anabolic and catabolic
498 processes in mutually opposing ways. In sensing the lack of nutrients, AMPK signals activate the
499 catabolic process while inhibiting the anabolic one. On the other hand, responding to nutrient
500 availability, mTORC1 activation upregulates anabolic metabolism and promotes cell growth.
501 Intriguingly, it is now known that both mTORC1 and AMPK are recruited to the lysosomal
502 surface for activation, which requires the scaffold Ragulator complex that consists of LAMTOR
503 subunits. We found that the Ragulator complex (LMTR-2, 3 and 5) is enriched at the lysosome

504 purified from WT worms using CTNS-1 but not LMP-1 Lyso-IP (Figure 6E), suggesting a
505 predominant association of the Ragulator complex with mature lysosomes, which could in turn
506 determine the preference of mTORC1 and AMPK activation at the lysosomal surface.
507 Alternatively, it would be also possible that the Ragulator complex carries a preference toward
508 CTNS-1/Cystinosin-containing lysosomes, which would infer the interaction between lysosomal
509 cysteine metabolism and mTORC1 signaling. Interestingly, previous studies show that
510 Cystinosin co-immunoprecipitates with the Ragulator complex in mammalian cells
511 (Andrzejewska et al., 2016), and in *Drosophila,* cysteine efflux from the lysosome via Cystinosin
512 antagonizes mTORC1 signaling and upregulates the tricarboxylic acid cycle (Jouandin et al.,
513 2022). Whether this inhibitory effect of lysosomal cysteine on mTORC1 is related to the
514 preferential interaction between the Ragulator complex and Cystinosin would be an interesting
515 question for future studies.
516
517 Both mTORC1 and AMPK have been implicated in the regulation of longevity across different
518 species, being intertwined with other longevity regulatory mechanisms (Savini et al., 2019). In
519 the long-lived *lipl-4 Tg* worms, the lysosomal enrichment of the Ragulator complex is increased
520 with LMP-1 Lyso-IP, which may be a result of the increased proportion of mature lysosomes
521 upon the induction of lysosomal lipolysis. At the same time, we could not rule out the possibility
522 that the increased enrichment of the Ragulator complex is a result of the induced level of
523 lysosomal CTNS-1/Cystinosin in the *lipl-4 Tg* worms. We found that with LMP-1 Lyso-IP, the
524 level of the CTNS-1/Cystinosin transporter is increased in the *lipl-4 Tg* worms, together with the
525 increase of several cysteine cathepsins (Figure 6F). Our previous studies found that
526 mitochondrial β-oxidation is increased in the *lipl-4 Tg* worms, leading to decreased triglyceride

527 storage (Ramachandran et al., 2019). The *lipl-4 Tg* worms also show an induced autophagy (Mak
528 et al., 2020). These phenotypes are the same as those observed in fruit flies with Cystinosin
529 overexpression (Jouandin et al., 2022). Considering the inhibitory effect of Cystinosin on
530 mTORC1 in fruit flies, the induction of Cystinosin in the *lipl-4 Tg* worms might reduce
531 mTORC1 signaling. In supporting this idea, our unpublished study shows that *lipl-4 Tg* does not
532 further enhance the lifespan extension of the *raga-1* mutant that has reduced mTORC1 signaling.
533 Furthermore, our study reveals the lysosomal enrichment of AMPK in the *lipl-4 Tg* worms, and
534 its requirement for the longevity effect (Figure 3C, 3D). On the other hand, the involvement of
535 lysosomal mTORC1 and AMPK signaling in regulating the longevity effect associated with
536 reduced insulin/IGF-1 signaling was not identified in the *daf-2(lf)* mutant. It would be interesting
537 for future studies to systemically profile lysosome-enriched proteomes in other longevity models,
538 such as caloric restriction, mild inhibition of mitochondrial respiration and germline deficiency,
539 using the same method, which would help understand the involvement of lysosomal metabolism
540 and signaling in these different longevity mechanisms.
541

542 **MATERIALS AND METHODS**

543

544 ***C. elegans* strains and maintenance**

545 The following strains were used in this study: N2, CB1370 *daf-2(e1370),* RB754 *aak-2(ok524)*,
546 *unc-76(e911)*, MCW953 *nre-1(hd20);lin-15b(hd126)*, MCW14 *raxIs3 [ges-1p::lipl-*
547 *4::SL2GFP]*, MCW859 *raxIs103[sur-5p:lmp-1::RFP-3×HA;unc-76(+)],* MCW935 *daf-*
548 *2(e1370);raxIs103[sur-5p:lmp-1::RFP-3×HA;unc-76(+)],* MCW923 *raxIs3[ges-1p::lipl-*
549 *4::SL2GFP];raxIs103[sur-5p:lmp-1::RFP-3×HA;unc-76(+)], MCW861 unc-*

550 *76(e911);raxEx311[Pmyo-3:lmp-1::RFP-3×HA;unc-76(+)],* MCW924 *unc-76(e911);*
551 *raxEx346[Pcol-12:lmp-1::RFP-3×HA;unc-76(+)],* MCW862 *unc-76(e911);raxEx312[Punc-*
552 *119:lmp-1::RFP-3×HA;unc-76(+)],* MCW914 *unc-76(e911);raxEx341[Pges-1:lmp-1::RFP-*
553 *3×HA;unc-76(+)],* MCW934 *raxIs118[sur-5p:ctns-1::RFP-3×HA;unc-76(+)].* The strains N2,
554 CB1370, and RB754 were obtained from *Caenorhabditis* Genetics Center (CGC). The strain
555 *unc-76(e911)* was obtained from Dr. Zheng Zhou's Lab. Other strains were generated in our lab.
556
557 *C. elegans* strains were maintained at 20˚C on standard NGM agar plates seeded with OP50
558 *E.coli* (HT115 *E. coli* for RNAi experiments) using standard protocols (Stiernagle, 2006) and
559 kept at least three generations without starvation before experiments.
560
561 **Molecular cloning and generating transgenics**
562 All the expression constructs were generated using Multisite Gateway System (Invitrogen) as
563 previously described (Mutlu et al., 2020). The *lmp-1* and *ctns-1* coding sequences were PCR-
564 amplified from *C. elegans* cDNA then inframe fused with RFP-3×HA, and all promoters were
565 PCR-amplified from *C. elegans* genomic DNA.
566
567 Transgenic strains were generated by microinjecting the day-1-adult germline of *unc-76(e911)*
568 worms with DNA mixture containing expression construct and *unc-76(+)* rescuing plasmid. For
569 integration strains, the stable extrachromosomal arrays were integrated with gamma irradiation
570 (4500 rads for in 5.9 minutes) and backcrossing to wild-type N2 at least 8 times.
571
572 **Lysosome immunoprecipitation (Lyso-IP)**

573 Lyso-IP is based on the method used in mammalian cells (Abu-Remaileh et al., 2017). Briefly,
574 transgenic strains stably expressing C-terminal RFP- and 3×HA-tagged lysosomal membrane
575 protein LMP-1 or CTNS-1 under whole-body *Psur-5* or tissue-specific promoters were
576 generated. Around 160,000 day-1-adult worms per genotype were collected, washed 3 times with
577 M9 buffer then washed 1 time with KPBS buffer (136 mM KCl, 10 mM KH_2PO_4). Worms in 2
578 ml KPBS were quickly homogenized with Dounce homogenizer on ice until no visible animals
579 were seen under the microscope. The lysate was centrifuged at 1000 g for 3 min at 4 ˚C to
580 remove debris and then the supernatant was incubated with anti-HA magnetic beads (Thermo
581 Fisher Scientific, cat. # 88837) for 6 minutes at 20 ˚C. The bound beads and flowthrough were
582 separated using a magnetic stand. The bound bead fraction was washed 4 times with cold KPBS.
583 The bound bead and flowthrough fractions were both used for LC/MS-based proteomics
584 analyses.
585
586 **LC/MS-based proteomic analyses**
587 The bound beads after wash were directly eluted in 100 µl of 5% SDS buffer and trypsin
588 digestion was carried out using S-Trap™ (Protifi, NY) as per manufacturer's protocol. For the
589 flow-through sample after IP, 100 µl sample was diluted in 5% SDS buffer and trypsin digestion
590 was carried out using S-Trap™. The peptide concentration was measured using the Pierce™
591 Quantitative Colorimetric Peptide Assay (Thermo Scientific cat. # 23275). The digested peptides
592 were subjected to simple C18 clean up using a C18 disk plug (3M Empore C18) and dried in a
593 speed vac. 1 µg of the peptide was used for LC-MS/MS analysis which was carried out using a
594 nano-LC 1200 system (Thermo Fisher Scientific, San Jose, CA) coupled to Orbitrap Fusion™
595 Lumos ETD mass spectrometer (Thermo Fisher Scientific, San Jose, CA). The peptides were

596 loaded on a two-column setup using a pre-column trap of 2 cm × 100 µm size (Reprosil-Pur
597 Basic C18 1.9 µm, Dr. Maisch GmbH, Germany) and a 5 cm × 75 µm analytical column
598 (Reprosil-Pur Basic C18 1.9 µm, Dr. Maisch GmbH, Germany) with a 75 min gradient of 5-28%
599 acetonitrile/0.1% formic acid at a flow rate of 750 nl/min. The eluted peptides were directly
600 electro-sprayed into mass spectrometer operated in the data-dependent acquisition (DDA) mode.
601 The full MS scan was acquired in Orbitrap in the range of 300-1400 m/z at 120,000 resolution
602 followed by top 30 MS2 in Ion Trap (AGC 5000, MaxIT 35 ms, HCD 28% collision energy)
603 with 15 sec dynamic exclusion time.
604
605 The raw files were searched using Mascot algorithm (Mascot 2.4, Matrix Science) against the
606 *Caenorhabditis elegans* NCBI refseq protein database in the Proteome Discoverer (PD 2.1,
607 Thermo Fisher) interface. The precursor mass tolerance was set to 20 ppm, fragment mass
608 tolerance to 0.5 Da, maximum of two missed cleavage was allowed. Dynamic modification of
609 oxidation on methionine, protein N-terminal Acetylation and deamidation (N/Q) was allowed.
610 The gene product inference and iBAQ-based quantification were carried out using the gpGrouper
611 algorithm (Saltzman et al., 2018). The iBAQ values were normalized to the fraction of total
612 protein iBAQ per experiment defined as 'iFOT (Fraction of total)'.
613
614 **Antibodies**
615 Anti-*C. elegans* LMP-1, HSP-60, CYP-33, SVQ-8 monoclonal antibodies were purchased
616 from Developmental Studies Hybridoma Bank (DHSB). Those antibodies were originally
617 generated by Dr. Michael L. Nonet's lab (Hadwiger et al., 2010). Anti-β-actin antibody (C4) was
618 purchased from Santa Cruz (sc-47778).

619

620 **Microscopy imaging**

621 Regular microscopy

622 Tissue-specific lyso-Tag expression example images (Figure 5A) were captured using Leica
623 DMi8 THUNDER Imaging Systems using 20× objective. Other microscopy images were
624 captured using Olympus FV3000 confocal microscopy system using 60× or 20× objective. *C.*
625 *elegans* were anesthetized in 1% sodium azide in M9 buffer and placed on 2% agarose pad
626 sandwiched between the glass microscopic slide and coverslip.

627

628 Fluorescence lifetime microscopy

629 L1 RNAi sensitive *nre-1(hd20);lin-15b(hd126)* worms were seeded on 3.5cm RNAi plates and
630 raised at 20°C for two days, and then around 20 worms each well were transferred to the 3.5cm
631 RNAi plates containing RNAi bacteria and 0.5 μM of LysoSensor Green DND-189
632 (Invitrogen™ L7535) and raised for 18h (in dark) at 20°C. The worms were imaged using ISS
633 Q2 Time-resolved Laser Scanning Confocal Nanoscope. The laser excitation wavelength was set
634 at 476nm and the 500-633nm emission filter was used to detect the LysoSenor Green signal. The
635 first pair of intestinal cells of each worm was imaged. The lifetimes of LysoSensor-containing
636 puncta were measured using ISS VistaVision software. The pH of the lysosome was then
637 calculated based on the LysoSensor lifetime-pH calibration curve.

638

639 **LysoSensor RNAi screen**

640 The primary screen was performed on 95 lysosomal-enriched candidates shared between the
641 LMP-1 and the CTNS-1 Lyso-IP proteomic profiling datasets. Each RNAi bacteria clone was

642 seeded onto 12-well RNAi plates containing 1 mM IPTG and allowed to dry. The dried plates
643 were then incubated at room temperature overnight to induce dsRNA expression. Synchronized
644 L1 *nre-1(hd20);lin-15b(hd126)* worms were seeded on 12-well RNAi plates and raised at 20 °C
645 for two days, and then around 30 worms each well were transferred to the RNAi plates
646 containing RNAi bacteria and 0.5 μM of LysoSensor Green DND-189. After 18 hours,
647 LysoSensor signals were examined by naked eyes using Nikon SMZ18 fluorescence stereo
648 microscope. The candidates with obvious LysoSensor alteration were selected for the secondary
649 LysosSensor RNAi screen. In the secondary screen, worms stained using LysoSensor Green
650 DND-189 were imaged by the FV3000 confocal laser scanning microscope (At least 15 animals
651 were measured in each condition). The changes in LysoSensor signals in the first pair of intestine
652 cells were quantified by ImageJ (including intensity, size, and number).
653
654 **Lysosome distribution quantification**
655 The quantification method was modified from previous publications on lysosomal distribution in
656 mammalian cell lines (Johnson et al., 2016; Willett et al., 2017). Images were first captured using
657 Olympus Fluoview software and imported into Matlab by Bio-Formats tool (Linkert et al., 2010).
658 Next, the cell membrane and nuclear membrane are outlined manually. The algorithm (code
659 included in Supplementary materials) determines the geometric center of the nucleus and radiates
660 at all angles to locate line segments between the nuclear and cell membrane. The line segments
661 are then evenly divided and circled to segment the cytosol into different regions. We calculate: 1.
662 The mean RFP fluorescence distribution across regions (normalized to the mean intensity of the
663 whole cell to avoid variations of RFP expression across cells) (Figure 4D, 4F); 2. The cumulative
664 intensity distribution from the most perinuclear region to the most peripheral region (normalized

665 to the overall intensity of the whole cell) (Supplementary Figure 2B, 2C). The algorithm requires
666 a convex shape of the cell, and most of the gut cells imaged meet this need.
667
668 **Lifespan assays**
669 Worms were synchronized by bleach-based egg preparation and subsequent starvation in M9
670 buffer for over 24 hours. Synchronized L1 worms were placed on the plates, and animals were
671 synchronized again by manual picking at mid L4 stage and marked as Day 0. Approximately 90-
672 120 worms were placed in three parallel plates for each condition. Worms are hence observed
673 and transferred to freshly made RNAi plates every other day. Animals are categorized as alive,
674 death (cessation of movement in response to platinum wire probing) or censored. The statistical
675 analyses were performed with the SPSS23 Kaplan-Meier survival function and the log-rank test.
676 GraphPad Prism 9 was used to graph the results.
677
678 **Structural stimulation by AlphaFold2**
679 The structure of R144.6 (UniProt: Q10000) was predicted by AlphaFold2 and downloaded from
680 The AlphaFold Protein Structure Database (https://alphafold.ebi.ac.uk/) (Jumper et al., 2021;
681 Varadi et al., 2022). The molecular graphics of the R144.6 structure was performed with UCSF
682 Chimera (Pettersen et al., 2004).
683
684 **Statistical methods**
685 Principal components analysis (PCA) was performed by R package Factextra (Le et al., 2008)
686 with the normalized iFOT abundance of proteins detected as the input. The Pearson correlation
687 matrices and coefficient (r) among replicates were generated by GraphPad Prism 9. The

688 unpaired, two-tailed t-tests for the multiple comparisons were used to calculate the p-values in
689 the correlation analyses by GraphPad Prism 9.
690
691 **Data availability**
692 The mass spectrometry data for protein identification have been deposited via the MASSIVE
693 repository (MSV000090909) to the Proteome X change Consortium
694 (http://proteomecentral.proteomexchange.org) with the dataset identifier PXD038865.
695 Analysis code for Figure 4 D, F and Figure S2 is included in Supplementary code.
696
697 **Conflict of Interest**
698 None declared.
699
700 **ACKNOWLEDGEMENTS**
701 We thank A. Dervisefendic and P. Svay for maintenance support; Mass Spectrometry Proteomics
702 Core of Baylor College of Medicine for mass spectrometry proteomic analysis; Z. Zhou (Baylor
703 College of Medicine) for sharing *unc-76(e911)* strain. Some strains were obtained from the
704 *Caenorhabditis* Genetics Center (CGC), which is funded by NIH Office of Research
705 Infrastructure Programs (P40 OD010440). M.C.W. is currently supported by Howard Hughes
706 Medical Institute, and Y.Y. is currently supported by National Natural Science Foundation of
707 China 32071146.
708
709 **AUTHOR CONTRIBUTIONS**

710 Y.Y., S.M.G., Y.G. and M.C.W. conceived the project and designed the experiments. Y.Y.,
711 S.M.G., Y.G., P.H., Q. Zhang, J.L., B.J. and S.Y.J. performed experiments. Q. Zhao conducted
712 the structural simulation. D.M.S. and M.A. help design Lyso-IP method in *C. elegans*. S.Y.J.
713 supervised mass spectrometry analysis. Y.Y., S.M.G., Y.G. and M.C.W. wrote the manuscript.
714 Y.Y., S.M.G., Y.G., Q. Zhang, M.A. and M.C.W. edited the manuscript.
715

716 **REFERENCE**

717

718 Abu-Remaileh, M., Wyant, G. A., Kim, C., Laqtom, N. N., Abbasi, M., Chan, S. H., Freinkman, E.,
719 & Sabatini, D. M. (2017). Lysosomal metabolomics reveals V-ATPase- and mTOR-
720 dependent regulation of amino acid efflux from lysosomes. *Science*, *358*(6364), 807-813.
721 https://doi.org/10.1126/science.aan6298
722 Andrzejewska, Z., Nevo, N., Thomas, L., Chhuon, C., Bailleux, A., Chauvet, V., Courtoy, P. J., Chol,
723 M., Guerrera, I. C., & Antignac, C. (2016). Cystinosin is a Component of the Vacuolar H+-
724 ATPase-Ragulator-Rag Complex Controlling Mammalian Target of Rapamycin Complex 1
725 Signaling. *J Am Soc Nephrol*, *27*(6), 1678-1688.
726 https://doi.org/10.1681/ASN.2014090937
727 Apfeld, J., O'Connor, G., McDonagh, T., DiStefano, P. S., & Curtis, R. (2004). The AMP-activated
728 protein kinase AAK-2 links energy levels and insulin-like signals to lifespan in *C. elegans*.
729 *Genes Dev*, *18*(24), 3004-3009. https://doi.org/10.1101/gad.1255404
730 Appelqvist, H., Waster, P., Kagedal, K., & Ollinger, K. (2013). The lysosome: from waste bag to
731 potential therapeutic target. *J Mol Cell Biol*, *5*(4), 214-226.
732 https://doi.org/10.1093/jmcb/mjt022
733 Ballabio, A., & Bonifacino, J. S. (2020). Lysosomes as dynamic regulators of cell and organismal
734 homeostasis. *Nature reviews Molecular cell biology*, *21*(2), 101-118.
735 https://doi.org/10.1038/s41580-019-0185-4
736 Ballabio, A., & Gieselmann, V. (2009). Lysosomal disorders: from storage to cellular damage.
737 *Biochim Biophys Acta*, *1793*(4), 684-696. https://doi.org/10.1016/j.bbamcr.2008.12.001
738 Braulke, T., & Bonifacino, J. S. (2009). Sorting of lysosomal proteins. *Biochimica Et Biophysica*
739 *Acta-Molecular Cell Research*, *1793*(4), 605-614.
740 https://doi.org/10.1016/j.bbamcr.2008.10.016
741 Brown, C. A., & Black, S. D. (1989). Membrane topology of mammalian cytochromes P-450 from
742 liver endoplasmic reticulum. Determination by trypsinolysis of phenobarbital-treated
743 microsomes. *J Biol Chem*, *264*(8), 4442-4449.
744 https://www.ncbi.nlm.nih.gov/pubmed/2925650
745 Castellano, B. M., Thelen, A. M., Moldavski, O., Feltes, M., van der Welle, R. E., Mydock-
746 McGrane, L., Jiang, X., van Eijkeren, R. J., Davis, O. B., Louie, S. M., Perera, R. M., Covey,

747 D. F., Nomura, D. K., Ory, D. S., & Zoncu, R. (2017). Lysosomal cholesterol activates
748 mTORC1 via an SLC38A9-Niemann-Pick C1 signaling complex. *Science*, *355*(6331), 1306-
749 1311. https://doi.org/10.1126/science.aag1417
750 Crighton, D., Wilkinson, S., O'Prey, J., Syed, N., Smith, P., Harrison, P. R., Gasco, M., Garrone, O.,
751 Crook, T., & Ryan, K. M. (2006). DRAM, a p53-induced modulator of autophagy, is critical
752 for apoptosis. *Cell*, *126*(1), 121-134. https://doi.org/10.1016/j.cell.2006.05.034
753 Cruciat, C. M., Ohkawara, B., Acebron, S. P., Karaulanov, E., Reinhard, C., Ingelfinger, D.,
754 Boutros, M., & Niehrs, C. (2010). Requirement of prorenin receptor and vacuolar H+-
755 ATPase-mediated acidification for Wnt signaling. *Science*, *327*(5964), 459-463.
756 https://doi.org/10.1126/science.1179802
757 Davidson, S. M., & Vander Heiden, M. G. (2017). Critical Functions of the Lysosome in Cancer
758 Biology. *Annu Rev Pharmacol Toxicol*, *57*, 481-507. https://doi.org/10.1146/annurev-
759 pharmtox-010715-103101
760 de Araujo, M. E. G., Naschberger, A., Furnrohr, B. G., Stasyk, T., Dunzendorfer-Matt, T., Lechner,
761 S., Welti, S., Kremser, L., Shivalingaiah, G., Offterdinger, M., Lindner, H. H., Huber, L. A.,
762 & Scheffzek, K. (2017). Crystal structure of the human lysosomal mTORC1 scaffold
763 complex and its impact on signaling. *Science*, *358*(6361), 377-381.
764 https://doi.org/10.1126/science.aao1583
765 De Franceschi, N., Hamidi, H., Alanko, J., Sahgal, P., & Ivaska, J. (2015). Integrin traffic - the
766 update. *J Cell Sci*, *128*(5), 839-852. https://doi.org/10.1242/jcs.161653
767 Diao, J., Liu, R., Rong, Y., Zhao, M., Zhang, J., Lai, Y., Zhou, Q., Wilz, L. M., Li, J., Vivona, S.,
768 Pfuetzner, R. A., Brunger, A. T., & Zhong, Q. (2015). ATG14 promotes membrane
769 tethering and fusion of autophagosomes to endolysosomes. *Nature*, *520*(7548), 563-
770 566. https://doi.org/10.1038/nature14147
771 Eapen, V. V., Swarup, S., Hoyer, M. J., Paulo, J. A., & Harper, J. W. (2021). Quantitative
772 proteomics reveals the selectivity of ubiquitin-binding autophagy receptors in the
773 turnover of damaged lysosomes by lysophagy. *Elife*, *10*.
774 https://doi.org/10.7554/eLife.72328
775 Eskelinen, E. L. (2006). Roles of LAMP-1 and LAMP-2 in lysosome biogenesis and autophagy.
776 *Mol Aspects Med*, *27*(5-6), 495-502. https://doi.org/10.1016/j.mam.2006.08.005
777 Ewan, L. C., Jopling, H. M., Jia, H. Y., Mittar, S., Bagherzadeh, A., Howell, G. J., Walker, J. H.,
778 Zachary, I. C., & Ponnambalam, S. (2006). Intrinsic tyrosine kinase activity is required for
779 vascular endothelial growth factor receptor 2 ubiquitination, sorting and degradation in
780 endothelial cells. *Traffic*, *7*(9), 1270-1282. https://doi.org/10.1111/j.1600-
781 0854.2006.00462.x
782 Fehrenbacher, N., & Jaattela, M. (2005). Lysosomes as targets for cancer therapy. *Cancer Res*,
783 *65*(8), 2993-2995. https://doi.org/10.1158/0008-5472.CAN-05-0476
784 Folick, A., Oakley, H. D., Yu, Y., Armstrong, E. H., Kumari, M., Sanor, L., Moore, D. D., Ortlund, E.
785 A., Zechner, R., & Wang, M. C. (2015). Lysosomal signaling molecules regulate longevity
786 in *Caenorhabditis elegans*. *Science*, *347*(6217), 83-86.
787 https://doi.org/10.1126/science.1258857
788 Forgac, M. (2007). Vacuolar ATPases: rotary proton pumps in physiology and pathophysiology.
789 *Nat Rev Mol Cell Biol*, *8*(11), 917-929. https://doi.org/10.1038/nrm2272

790 Gahl, W. A., Bashan, N., Tietze, F., Bernardini, I., & Schulman, J. D. (1982). Cystine transport is
791 defective in isolated leukocyte lysosomes from patients with cystinosis. *Science*,
792 *217*(4566), 1263-1265. https://doi.org/10.1126/science.7112129
793 Gallet, A., & Therond, P. P. (2005). Temporal modulation of the Hedgehog morphogen gradient
794 by a patched-dependent targeting to lysosomal compartment. *Developmental Biology*,
795 *277*(1), 51-62. https://doi.org/10.1016/j.ydbio.2004.09.005
796 Gao, Y., Chen, Y., Zhan, S., Zhang, W., Xiong, F., & Ge, W. (2017). Comprehensive proteome
797 analysis of lysosomes reveals the diverse function of macrophages in immune
798 responses. *Oncotarget*, *8*(5), 7420-7440. https://doi.org/10.18632/oncotarget.14558
799 Grant, B., & Hirsh, D. (1999). Receptor-mediated endocytosis in the *Caenorhabditis elegans*
800 oocyte. *Mol Biol Cell*, *10*(12), 4311-4326. https://doi.org/10.1091/mbc.10.12.4311
801 Graves, A. R., Curran, P. K., Smith, C. L., & Mindell, J. A. (2008). The Cl-/H+ antiporter ClC-7 is the
802 primary chloride permeation pathway in lysosomes. *Nature*, *453*(7196), 788-792.
803 https://doi.org/10.1038/nature06907
804 Hadwiger, G., Dour, S., Arur, S., Fox, P., & Nonet, M. L. (2010). A monoclonal antibody toolkit for
805 *C. elegans*. *PLoS One*, *5*(4), e10161. https://doi.org/10.1371/journal.pone.0010161
806 Hansen, M., Rubinsztein, D. C., & Walker, D. W. (2018). Autophagy as a promoter of longevity:
807 insights from model organisms. *Nat Rev Mol Cell Biol*, *19*(9), 579-593.
808 https://doi.org/10.1038/s41580-018-0033-y
809 Hartl, F. U., Martin, J., & Neupert, W. (1992). Protein folding in the cell: the role of molecular
810 chaperones Hsp70 and Hsp60. *Annu Rev Biophys Biomol Struct*, *21*, 293-322.
811 https://doi.org/10.1146/annurev.bb.21.060192.001453
812 Itakura, E., Kishi-Itakura, C., & Mizushima, N. (2012). The hairpin-type tail-anchored SNARE
813 syntaxin 17 targets to autophagosomes for fusion with endosomes/lysosomes. *Cell*,
814 *151*(6), 1256-1269. https://doi.org/10.1016/j.cell.2012.11.001
815 Ivanov, A., Pawlikowski, J., Manoharan, I., van Tuyn, J., Nelson, D. M., Rai, T. S., Shah, P. P.,
816 Hewitt, G., Korolchuk, V. I., Passos, J. F., Wu, H., Berger, S. L., & Adams, P. D. (2013).
817 Lysosome-mediated processing of chromatin in senescence. *J Cell Biol*, *202*(1), 129-143.
818 https://doi.org/10.1083/jcb.201212110
819 Johnson, D. E., Ostrowski, P., Jaumouille, V., & Grinstein, S. (2016). The position of lysosomes
820 within the cell determines their luminal pH. *J Cell Biol*, *212*(6), 677-692.
821 https://doi.org/10.1083/jcb.201507112
822 Jonas, A. J., Greene, A. A., Smith, M. L., & Schneider, J. A. (1982). Cystine accumulation and loss
823 in normal, heterozygous, and cystinotic fibroblasts. *Proc Natl Acad Sci U S A*, *79*(14),
824 4442-4445. https://doi.org/10.1073/pnas.79.14.4442
825 Jouandin, P., Marelja, Z., Shih, Y. H., Parkhitko, A. A., Dambowsky, M., Asara, J. M., Nemazanyy,
826 I., Dibble, C. C., Simons, M., & Perrimon, N. (2022). Lysosomal cystine mobilization
827 shapes the response of TORC1 and tissue growth to fasting. *Science*, *375*(6582),
828 eabc4203. https://doi.org/10.1126/science.abc4203
829 Jumper, J., Evans, R., Pritzel, A., Green, T., Figurnov, M., Ronneberger, O., Tunyasuvunakool, K.,
830 Bates, R., Zidek, A., Potapenko, A., Bridgland, A., Meyer, C., Kohl, S. A. A., Ballard, A. J.,
831 Cowie, A., Romera-Paredes, B., Nikolov, S., Jain, R., Adler, J., . . . Hassabis, D. (2021).
832 Highly accurate protein structure prediction with AlphaFold. *Nature*, *596*(7873), 583-
833 589. https://doi.org/10.1038/s41586-021-03819-2

834 Kalatzis, V., Cherqui, S., Antignac, C., & Gasnier, B. (2001). Cystinosin, the protein defective in
835 cystinosis, is a H(+)-driven lysosomal cystine transporter. *EMBO J*, *20*(21), 5940-5949.
836 https://doi.org/10.1093/emboj/20.21.5940
837 Kane, P. M. (1995). Disassembly and reassembly of the yeast vacuolar H(+)-ATPase *in vivo*. *J Biol*
838 *Chem*, *270*(28), 17025-17032. https://www.ncbi.nlm.nih.gov/pubmed/7622524
839 Kang, D. S., Tian, X., & Benovic, J. L. (2014). Role of beta-arrestins and arrestin domain-
840 containing proteins in G protein-coupled receptor trafficking. *Curr Opin Cell Biol*, *27*, 63-
841 71. https://doi.org/10.1016/j.ceb.2013.11.005
842 Kenyon, C., Chang, J., Gensch, E., Rudner, A., & Tabtiang, R. (1993). A *C. elegans* mutant that
843 lives twice as long as wild type. *Nature*, *366*(6454), 461-464.
844 https://doi.org/10.1038/366461a0
845 Khan, A. S., & Frigo, D. E. (2017). A spatiotemporal hypothesis for the regulation, role, and
846 targeting of AMPK in prostate cancer. *Nat Rev Urol*, *14*(3), 164-180.
847 https://doi.org/10.1038/nrurol.2016.272
848 Lapierre, L. R., Gelino, S., Melendez, A., & Hansen, M. (2011). Autophagy and lipid metabolism
849 coordinately modulate life span in germline-less *C. elegans*. *Curr Biol*, *21*(18), 1507-1514.
850 https://doi.org/10.1016/j.cub.2011.07.042
851 Laqtom, N. N., Dong, W., Medoh, U. N., Cangelosi, A. L., Dharamdasani, V., Chan, S. H., Kunchok,
852 T., Lewis, C. A., Heinze, I., Tang, R., Grimm, C., Dang Do, A. N., Porter, F. D., Ori, A.,
853 Sabatini, D. M., & Abu-Remaileh, M. (2022). CLN3 is required for the clearance of
854 glycerophosphodiesters from lysosomes. *Nature*, *609*(7929), 1005-1011.
855 https://doi.org/10.1038/s41586-022-05221-y
856 Lawrence, R. E., & Zoncu, R. (2019). The lysosome as a cellular centre for signalling, metabolism
857 and quality control. *Nat Cell Biol*, *21*(2), 133-142. https://doi.org/10.1038/s41556-018-
858 0244-7
859 Le, S., Josse, J., & Husson, F. (2008). FactoMineR: An R package for multivariate analysis. *Journal*
860 *of statistical software*, *25*(1), 1-18. https://doi.org/10.18637/jss.v025.i01
861 Leger-Silvestre, I., Caffrey, J. M., Dawaliby, R., Alvarez-Arias, D. A., Gas, N., Bertolone, S. J.,
862 Gleizes, P. E., & Ellis, S. R. (2005). Specific Role for Yeast Homologs of the Diamond
863 Blackfan Anemia-associated Rps19 Protein in Ribosome Synthesis. *J Biol Chem*, *280*(46),
864 38177-38185. https://doi.org/10.1074/jbc.M506916200
865 Li, R. J., Xu, J., Fu, C., Zhang, J., Zheng, Y. G., Jia, H., & Liu, J. O. (2016). Regulation of mTORC1 by
866 lysosomal calcium and calmodulin. *Elife*, *5*. https://doi.org/10.7554/eLife.19360
867 Linkert, M., Rueden, C. T., Allan, C., Burel, J. M., Moore, W., Patterson, A., Loranger, B., Moore,
868 J., Neves, C., Macdonald, D., Tarkowska, A., Sticco, C., Hill, E., Rossner, M., Eliceiri, K. W.,
869 & Swedlow, J. R. (2010). Metadata matters: access to image data in the real world. *J Cell*
870 *Biol*, *189*(5), 777-782. https://doi.org/10.1083/jcb.201004104
871 Lubke, T., Lobel, P., & Sleat, D. E. (2009). Proteomics of the lysosome. *Biochim Biophys Acta*,
872 *1793*(4), 625-635. https://doi.org/10.1016/j.bbamcr.2008.09.018
873 Ma, Z., Thomas, K. S., Webb, D. J., Moravec, R., Salicioni, A. M., Mars, W. M., & Gonias, S. L.
874 (2002). Regulation of Rac1 activation by the low density lipoprotein receptor-related
875 protein. *J Cell Biol*, *159*(6), 1061-1070. https://doi.org/10.1083/jcb.200207070
876 Mak, K. H., Zhao, Q., Hu, P.-W., Au-Yeung, C.-L., Yang, J., Duraine, L., Yu, Y., Abu-Remaileh, M.,
877 Sabatini, D., Wang, J. D., & Wang, M. C. (2020). Lysosomal nucleotide metabolism

878 regulates ER proteostasis through mTOR signaling. *bioRxiv*, 2020.2004.2018.048561.
879 https://doi.org/10.1101/2020.04.18.048561
880 Markmann, S., Krambeck, S., Hughes, C. J., Mirzaian, M., Aerts, J. M., Saftig, P., Schweizer, M.,
881 Vissers, J. P., Braulke, T., & Damme, M. (2017). Quantitative Proteome Analysis of
882 Mouse Liver Lysosomes Provides Evidence for Mannose 6-phosphate-independent
883 Targeting Mechanisms of Acid Hydrolases in Mucolipidosis II. *Mol Cell Proteomics*, *16*(3),
884 438-450. https://doi.org/10.1074/mcp.M116.063636
885 Martins, R., Lithgow, G. J., & Link, W. (2016). Long live FOXO: unraveling the role of FOXO
886 proteins in aging and longevity. *Aging Cell*, *15*(2), 196-207.
887 https://doi.org/10.1111/acel.12427
888 Mayer, M. P. (2010). Gymnastics of molecular chaperones. *Mol Cell*, *39*(3), 321-331.
889 https://doi.org/10.1016/j.molcel.2010.07.012
890 McGuire, C. M., & Forgac, M. (2018). Glucose starvation increases V-ATPase assembly and
891 activity in mammalian cells through AMP kinase and phosphatidylinositide 3-kinase/Akt
892 signaling. *J Biol Chem*, *293*(23), 9113-9123. https://doi.org/10.1074/jbc.RA117.001327
893 Mijaljica, D., & Devenish, R. J. (2013). Nucleophagy at a glance. *J Cell Sci*, *126*(Pt 19), 4325-4330.
894 https://doi.org/10.1242/jcs.133090
895 Mutlu, A. S., Gao, S. M., Zhang, H., & Wang, M. C. (2020). Olfactory specificity regulates lipid
896 metabolism through neuroendocrine signaling in *Caenorhabditis elegans*. *Nature*
897 *communications*, *11*(1), 1-15. https://doi.org/10.1038/s41467-020-15296-8
898 Nakae, I., Fujino, T., Kobayashi, T., Sasaki, A., Kikko, Y., Fukuyama, M., Gengyo-Ando, K., Mitani,
899 S., Kontani, K., & Katada, T. (2010). The arf-like GTPase Arl8 mediates delivery of
900 endocytosed macromolecules to lysosomes in *Caenorhabditis elegans*. *Mol Biol Cell*,
901 *21*(14), 2434-2442. https://doi.org/10.1091/mbc.E09-12-1010
902 Navarro-Romero, A., Montpeyo, M., & Martinez-Vicente, M. (2020). The Emerging Role of the
903 Lysosome in Parkinson's Disease. *Cells*, *9*(11). https://doi.org/10.3390/cells9112399
904 Nicoli, E. R., Weston, M. R., Hackbarth, M., Becerril, A., Larson, A., Zein, W. M., Baker, P. R., 2nd,
905 Burke, J. D., Dorward, H., Davids, M., Huang, Y., Adams, D. R., Zerfas, P. M., Chen, D.,
906 Markello, T. C., Toro, C., Wood, T., Elliott, G., Vu, M., . . . Malicdan, M. C. V. (2019).
907 Lysosomal Storage and Albinism Due to Effects of a De Novo CLCN7 Variant on
908 Lysosomal Acidification. *Am J Hum Genet*, *104*(6), 1127-1138.
909 https://doi.org/10.1016/j.ajhg.2019.04.008
910 Nishimura, T., Kaizuka, T., Cadwell, K., Sahani, M. H., Saitoh, T., Akira, S., Virgin, H. W., &
911 Mizushima, N. (2013). FIP200 regulates targeting of Atg16L1 to the isolation membrane.
912 *EMBO Rep*, *14*(3), 284-291. https://doi.org/10.1038/embor.2013.6
913 Nixon, R. A., & Cataldo, A. M. (2006). Lysosomal system pathways: genes to neurodegeneration
914 in Alzheimer's disease. *J Alzheimers Dis*, *9*(3 Suppl), 277-289.
915 https://doi.org/10.3233/jad-2006-9s331
916 Pettersen, E. F., Goddard, T. D., Huang, C. C., Couch, G. S., Greenblatt, D. M., Meng, E. C., &
917 Ferrin, T. E. (2004). UCSF Chimera--a visualization system for exploratory research and
918 analysis. *J Comput Chem*, *25*(13), 1605-1612. https://doi.org/10.1002/jcc.20084
919 Platt, F. M., Boland, B., & van der Spoel, A. C. (2012). The cell biology of disease: lysosomal
920 storage disorders: the cellular impact of lysosomal dysfunction. *J Cell Biol*, *199*(5), 723-
921 734. https://doi.org/10.1083/jcb.201208152

922 Popovic, D., & Dikic, I. (2014). TBC1D5 and the AP2 complex regulate ATG9 trafficking and
923 initiation of autophagy. *EMBO Rep*, *15*(4), 392-401.
924 https://doi.org/10.1002/embr.201337995
925 Pu, J., Guardia, C. M., Keren-Kaplan, T., & Bonifacino, J. S. (2016). Mechanisms and functions of
926 lysosome positioning. *J Cell Sci*, *129*(23), 4329-4339. https://doi.org/10.1242/jcs.196287
927 Ramachandran, P. V., Savini, M., Folick, A. K., Hu, K., Masand, R., Graham, B. H., & Wang, M. C.
928 (2019). Lysosomal Signaling Promotes Longevity by Adjusting Mitochondrial Activity. *Dev*
929 *Cell*, *48*(5), 685-696 e685. https://doi.org/10.1016/j.devcel.2018.12.022
930 Ratto, E., Chowdhury, S. R., Siefert, N. S., Schneider, M., Wittmann, M., Helm, D., & Palm, W.
931 (2022). Direct control of lysosomal catabolic activity by mTORC1 through regulation of
932 V-ATPase assembly. *Nat Commun*, *13*(1), 4848. https://doi.org/10.1038/s41467-022-
933 32515-6
934 Rebsamen, M., Pochini, L., Stasyk, T., de Araujo, M. E., Galluccio, M., Kandasamy, R. K., Snijder,
935 B., Fauster, A., Rudashevskaya, E. L., Bruckner, M., Scorzoni, S., Filipek, P. A., Huber, K.
936 V., Bigenzahn, J. W., Heinz, L. X., Kraft, C., Bennett, K. L., Indiveri, C., Huber, L. A., &
937 Superti-Furga, G. (2015). SLC38A9 is a component of the lysosomal amino acid sensing
938 machinery that controls mTORC1. *Nature*, *519*(7544), 477-481.
939 https://doi.org/10.1038/nature14107
940 Saltzman, A. B., Leng, M., Bhatt, B., Singh, P., Chan, D. W., Dobrolecki, L., Chandrasekaran, H.,
941 Choi, J. M., Jain, A., Jung, S. Y., Lewis, M. T., Ellis, M. J., & Malovannaya, A. (2018).
942 gpGrouper: A Peptide Grouping Algorithm for Gene-Centric Inference and Quantitation
943 of Bottom-Up Proteomics Data. *Mol Cell Proteomics*, *17*(11), 2270-2283.
944 https://doi.org/10.1074/mcp.TIR118.000850
945 Savini, M., Folick, A., Lee, Y. T., Jin, F., Cuevas, A., Tillman, M. C., Duffy, J. D., Zhao, Q., Neve, I.
946 A., Hu, P. W., Yu, Y., Zhang, Q., Ye, Y., Mair, W. B., Wang, J., Han, L., Ortlund, E. A., &
947 Wang, M. C. (2022). Lysosome lipid signalling from the periphery to neurons regulates
948 longevity. *Nat Cell Biol*, *24*(6), 906-916. https://doi.org/10.1038/s41556-022-00926-8
949 Savini, M., Zhao, Q., & Wang, M. C. (2019). Lysosomes: Signaling Hubs for Metabolic Sensing
950 and Longevity. *Trends Cell Biol*, *29*(11), 876-887.
951 https://doi.org/10.1016/j.tcb.2019.08.008
952 Schroder, B. A., Wrocklage, C., Hasilik, A., & Saftig, P. (2010). The proteome of lysosomes.
953 *Proteomics*, *10*(22), 4053-4076. https://doi.org/10.1002/pmic.201000196
954 Snyder, J. C., Rochelle, L. K., Lyerly, H. K., Caron, M. G., & Barak, L. S. (2013). Constitutive
955 Internalization of the Leucine-rich G Protein-coupled Receptor-5 (LGR5) to the Trans-
956 Golgi Network. *Journal of Biological Chemistry*, *288*(15), 10286-10297.
957 https://doi.org/10.1074/jbc.M112.447540
958 Stiernagle, T. (2006). Maintenance of *C. elegans*. *WormBook*, 1-11.
959 https://doi.org/10.1895/wormbook.1.101.1
960 Stransky, L. A., & Forgac, M. (2015). Amino Acid Availability Modulates Vacuolar H+-ATPase
961 Assembly. *J Biol Chem*, *290*(45), 27360-27369.
962 https://doi.org/10.1074/jbc.M115.659128
963 Sugiura, T., Iga, T., Asai, T., & Mizokami, K. (1989). [Studies on diameter distribution of axons in
964 the optic pathway in human glaucoma]. *Nippon Ganka Gakkai Zasshi*, *93*(11), 1075-
965 1080. https://www.ncbi.nlm.nih.gov/pubmed/2603855

966 Sun, Y., Li, M., Zhao, D., Li, X., Yang, C., & Wang, X. (2020). Lysosome activity is modulated by
967 multiple longevity pathways and is important for lifespan extension in *C. elegans*. *Elife*,
968 *9*, e55745. https://doi.org/10.7554/eLife.55745
969 Turk, V., Stoka, V., Vasiljeva, O., Renko, M., Sun, T., Turk, B., & Turk, D. (2012). Cysteine
970 cathepsins: from structure, function and regulation to new frontiers. *Biochim Biophys*
971 *Acta*, *1824*(1), 68-88. https://doi.org/10.1016/j.bbapap.2011.10.002
972 Varadi, M., Anyango, S., Deshpande, M., Nair, S., Natassia, C., Yordanova, G., Yuan, D., Stroe, O.,
973 Wood, G., Laydon, A., Zidek, A., Green, T., Tunyasuvunakool, K., Petersen, S., Jumper, J.,
974 Clancy, E., Green, R., Vora, A., Lutfi, M., . . . Velankar, S. (2022). AlphaFold Protein
975 Structure Database: massively expanding the structural coverage of protein-sequence
976 space with high-accuracy models. *Nucleic Acids Res*, *50*(D1), D439-D444.
977 https://doi.org/10.1093/nar/gkab1061
978 Vasu, S., Shah, S., Orjalo, A., Park, M., Fischer, W. H., & Forbes, D. J. (2001). Novel vertebrate
979 nucleoporins Nup133 and Nup160 play a role in mRNA export. *J Cell Biol*, *155*(3), 339-
980 354. https://doi.org/10.1083/jcb.200108007
981 Wang, M. C., O'Rourke, E. J., & Ruvkun, G. (2008). Fat metabolism links germline stem cells and
982 longevity in *C. elegans*. *Science*, *322*(5903), 957-960.
983 https://doi.org/10.1126/science.1162011
984 Wang, S., Tsun, Z. Y., Wolfson, R. L., Shen, K., Wyant, G. A., Plovanich, M. E., Yuan, E. D., Jones,
985 T. D., Chantranupong, L., Comb, W., Wang, T., Bar-Peled, L., Zoncu, R., Straub, C., Kim,
986 C., Park, J., Sabatini, B. L., & Sabatini, D. M. (2015). Metabolism. Lysosomal amino acid
987 transporter SLC38A9 signals arginine sufficiency to mTORC1. *Science*, *347*(6218), 188-
988 194. https://doi.org/10.1126/science.1257132
989 Webb, B. A., Aloisio, F. M., Charafeddine, R. A., Cook, J., Wittmann, T., & Barber, D. L. (2021).
990 pHLARE: a new biosensor reveals decreased lysosome pH in cancer cells. *Mol Biol Cell*,
991 *32*(2), 131-142. https://doi.org/10.1091/mbc.E20-06-0383
992 Willett, R., Martina, J. A., Zewe, J. P., Wills, R., Hammond, G. R. V., & Puertollano, R. (2017).
993 TFEB regulates lysosomal positioning by modulating TMEM55B expression and JIP4
994 recruitment to lysosomes. *Nat Commun*, *8*(1), 1580. https://doi.org/10.1038/s41467-
995 017-01871-z
996 Wyant, G. A., Abu-Remaileh, M., Wolfson, R. L., Chen, W. W., Freinkman, E., Danai, L. V., Vander
997 Heiden, M. G., & Sabatini, D. M. (2017). mTORC1 Activator SLC38A9 Is Required to Efflux
998 Essential Amino Acids from Lysosomes and Use Protein as a Nutrient. *Cell*, *171*(3), 642-
999 654 e612. https://doi.org/10.1016/j.cell.2017.09.046
1000 Zhang, C. S., Jiang, B., Li, M., Zhu, M., Peng, Y., Zhang, Y. L., Wu, Y. Q., Li, T. Y., Liang, Y., Lu, Z.,
1001 Lian, G., Liu, Q., Guo, H., Yin, Z., Ye, Z., Han, J., Wu, J. W., Yin, H., Lin, S. Y., & Lin, S. C.
1002 (2014). The lysosomal v-ATPase-Ragulator complex is a common activator for AMPK and
1003 mTORC1, acting as a switch between catabolism and anabolism. *Cell Metab*, *20*(3), 526-
1004 540. https://doi.org/10.1016/j.cmet.2014.06.014
1005

1006 **FIGURES AND FIGURE LEGENDS**

1007

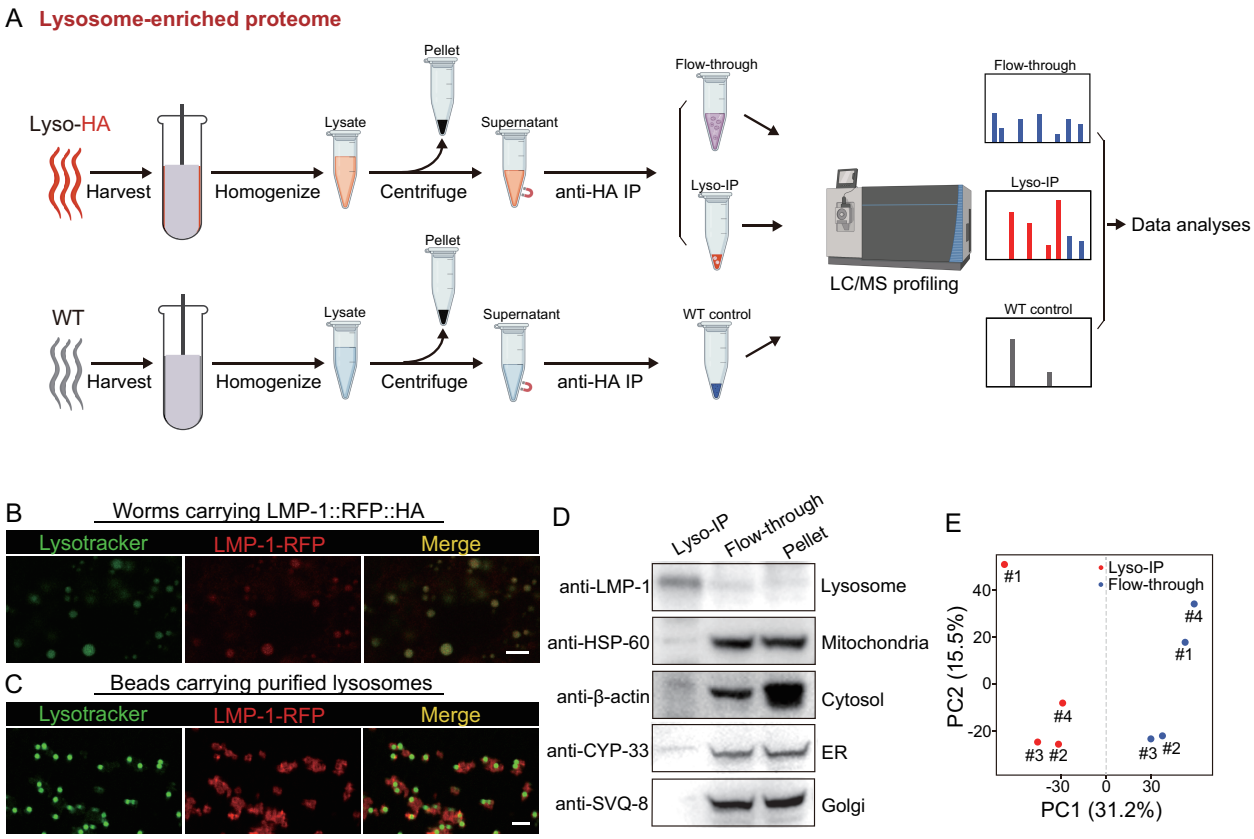

Figure 1. Rapid lysosome isolation coupled with proteomic profiling

(**A**) Schematic of the workflow for immunoprecipitation-based lysosome purification (Lyso-IP) and mass-spectrometry based proteomic profiling to identify lysosome-enriched proteomes in *C. elegans.*

(**B**) Example images of transgenic strains carrying LMP-1 Lyso-Tag (LMP-1::RFP-3×HA) with LysoTracker staining to mark lysosomes *in vivo*. Scale bar=5 µm.

(**C**) Example images of beads carrying purified lysosomes from Lyso-IP with LysoTracker staining to mark intact lysosomes *in vitro.* Scale bar=5 µm.

(**D**) Western blot for protein markers of different subcellular compartments using purified lysosomes (Lyso-IP), paired non-lysosomal fractions (Flow-through) or Pellet.

(**E**) PCA analysis of four independent biological replicates of Lyso-IP and Flow-through samples.

1021

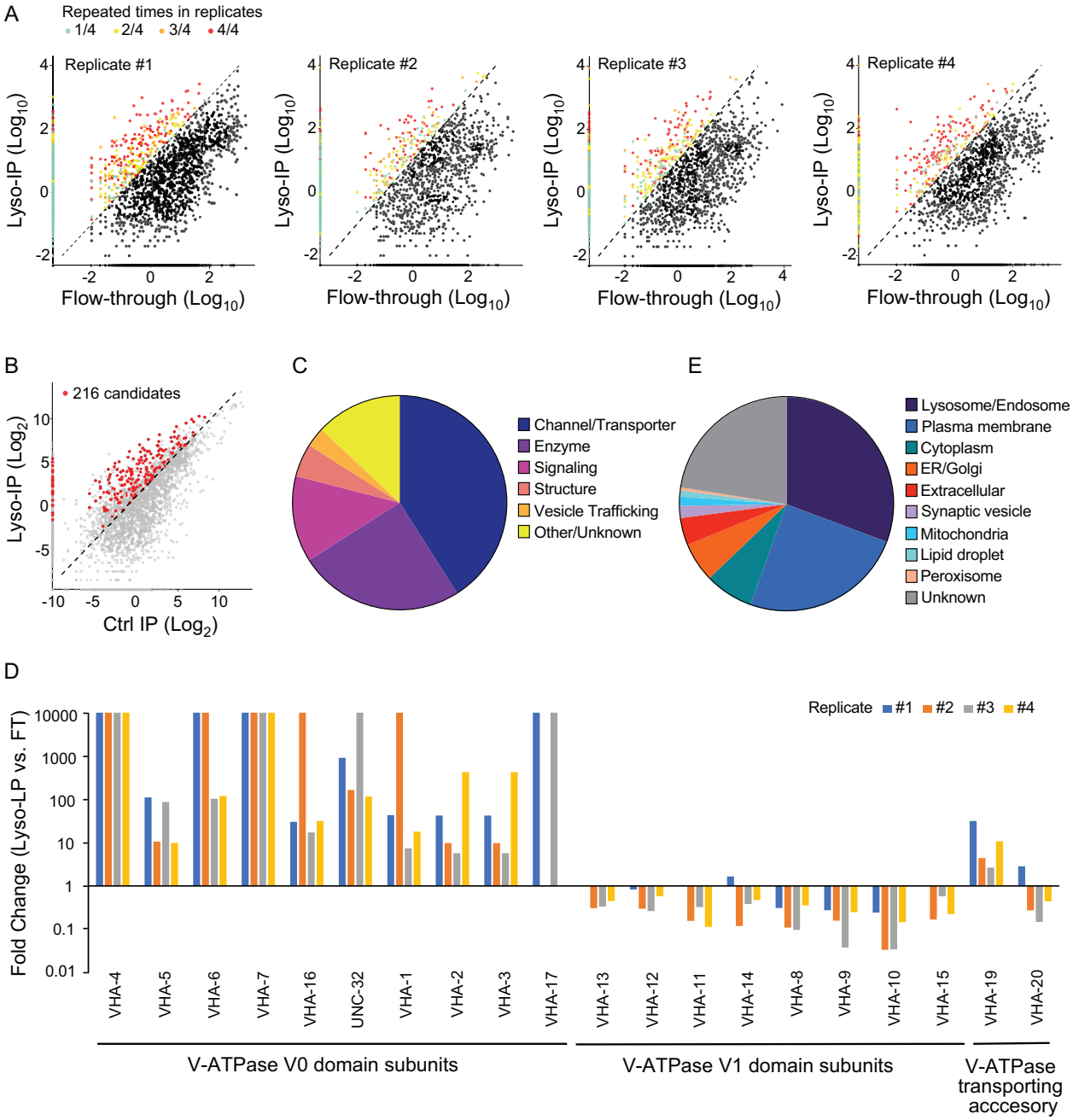

1022

1023 **Figure 2. Systemic view of lysosome-enriched proteome**

1024 (**A**) Scatter plots showing candidate selection from four independent biological replicates in

1025 proteomics analyses. Proteins with at least 10-fold higher levels in Lyso-IP samples than in flow-

1026 through controls are highlighted with different colors based on repeated times in four replicates.

1027 (**B**) Scatter plot showing candidate selection with normalization to non-tagged controls using
1028 wild-type worms. 216 proteins with over 2-fold higher levels in Lyso-IP samples than in non-
1029 tagged controls are highlighted in red.
1030 (**C**) Pie chart showing molecular function categories of lysosome-enriched proteins.
1031 (**D**) The lysosomal enrichment ratio (Lyso-IP vs FT) for each subunit of lysosomal vacuolar
1032 ATPase (v-ATPase) in four independent replicates is shown.
1033 (**E)** Pie chart showing subcellular location categories of lysosome-enriched proteins.
1034

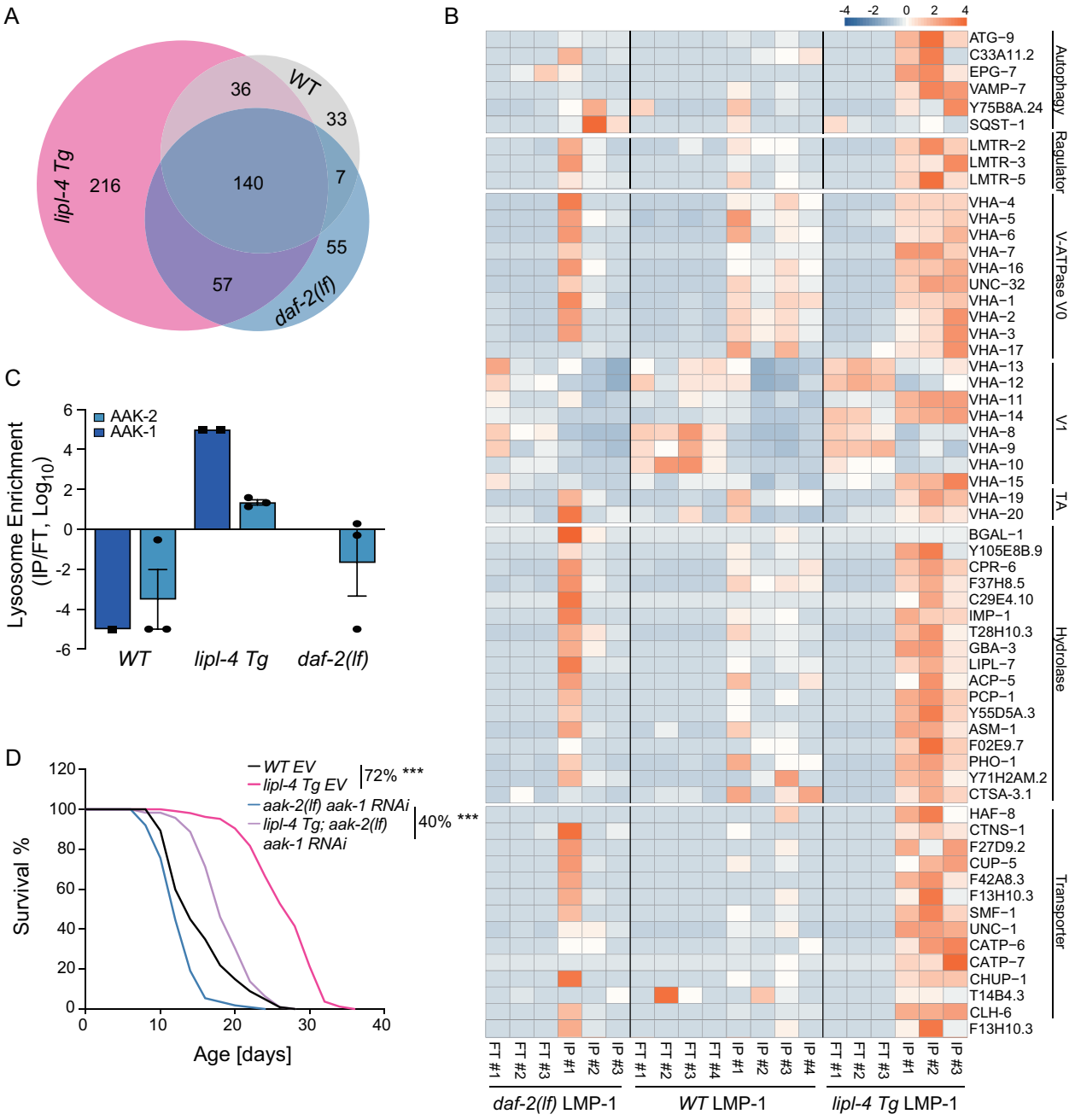

1035

1036 **Figure 3. Lysosome-enriched proteome associated with longevity**

1037 (**A**) Venn diagram showing overlaps among lysosome-enriched proteomes from wild-type (WT),

1038 *lipl-4 Tg* and *daf-2(lf)* worms.

1039 (**B**) Normalized protein levels (z-score across samples) of autophagy-related components,

1040 mTORC1 signaling factors, lysosomal v-ATPase V0, V1 and transporting accessory (TA)

1041 subunits, lysosomal hydrolases and transporter proteins from LMP-1 Lyso-IP proteomic analyses

1042 of WT, *lipl-4 Tg* and *daf-2(lf)*) worms.

1043 (**C**) The lysosomal enrichment ratio (Lyso-IP vs FT) for two homologs of AMPK catalytic

1044 subunits, AAK-1 and AAK-2 in WT, *lipl-4 Tg* and *daf-2(lf)*) worms.

1045 (**D**) Reduction of AMPK using the loss-of-function mutant of *aak-2, aak-2(lf)* together with *aak-*

1046 *1* RNAi knockdown reduces the lifespan extension in the *lipl-4 Tg* worms from 72% to 40%. ***

1047 $p<0.001$ by Log-rank test. The lifespan data are also in supplementary table 3.

1048

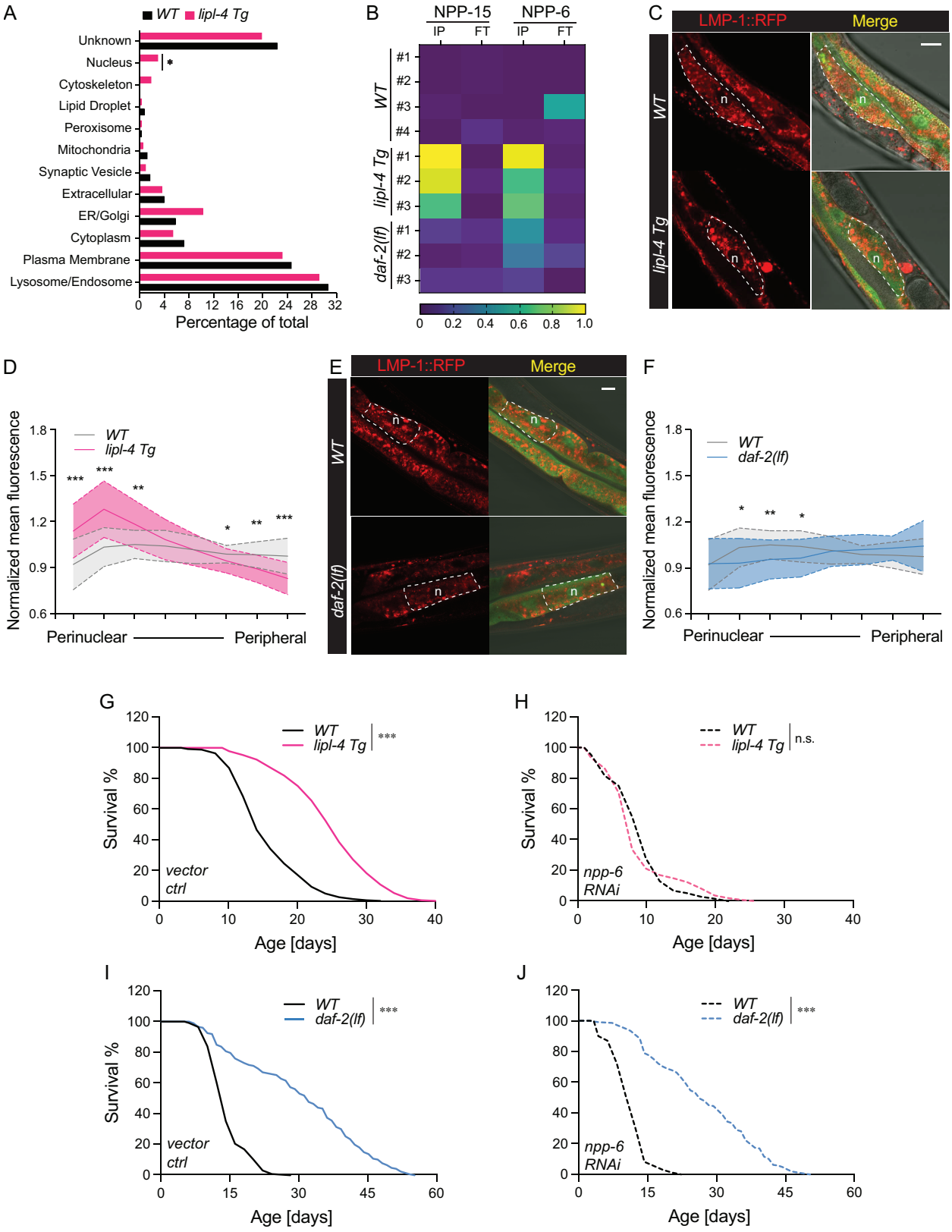

1049

1050 **Figure 4. Enhanced lysosome-nucleus interaction mediating longevity**

1051 **(A)** The percentage of proteins with different subcellular localization is compared between
1052 lysosome-enriched proteomes from WT and *lipl-4 Tg* worms. * p=0.019 by 2-sample test for
1053 equality of proportions.
1054 **(B)** Heatmap showing the average levels of nucleoporin proteins NPP-6 and NPP-15 in Lyso-IP
1055 (IP) and flow-through (FT) samples from WT, *lipl-4 Tg* and *daf-2(lf)* worms.
1056 **(C, E)** Representative images of intestinal cells in WT, *lipl-4 Tg* (**C**) and *daf-2(lf)* (**E**) worms
1057 carrying LMP-1::RFP-3×HA and nucleus-enriched GFP, showing the accumulation of
1058 lysosomes around the perinuclear region in the *lipl-4 Tg* but not *daf-2(lf)* worms. Dashed lines
1059 circle intestinal cells and n marks the nucleus. Scale bar=20 μm.
1060 **(D, F)** Line graph showing the spatial distribution of lysosomes from the nuclear to peripheral
1061 region quantified by normalized regional RFP fluorescence signals in intestinal cells of WT, *lipl-*
1062 *4 Tg* (**D**) and *daf-2(lf)* (**F**) worms. N =50 WT /33 *lipl-4 Tg*, 33 WT/ 28 *daf-2(lf)*. Data are
1063 represented as mean ± SD. p values for (D) (from left to right): 1.23×10^{-7}, 2.25×10^{-5}, 0.00322,
1064 0.368, 0.273, 0.0447, 0.00268, 1.20×10^{-5}; p values for (F) (from left to right): 0.633, 0.0211,
1065 0.00259, 0.0359, 0.767, 0.151, 0.106, 0.0671.
1066 **(G-H)** *lipl-4 Tg* worms show lifespan extension compared to WT worms (**G**), which is fully
1067 suppressed by RNAi knockdown of *npp-6* (**H**). ***$p<0.001$, n.s. $p>0.05$ by Log-rank test.
1068 **(I-J)** *daf-2(lf)* worms show lifespan extension compared to WT worms (**I**), which is not affected
1069 by *npp-6* RNAi knockdown (**J**). ***$p<0.001$ by Log-rank test. The lifespan data are also in
1070 supplementary table 3.
1071

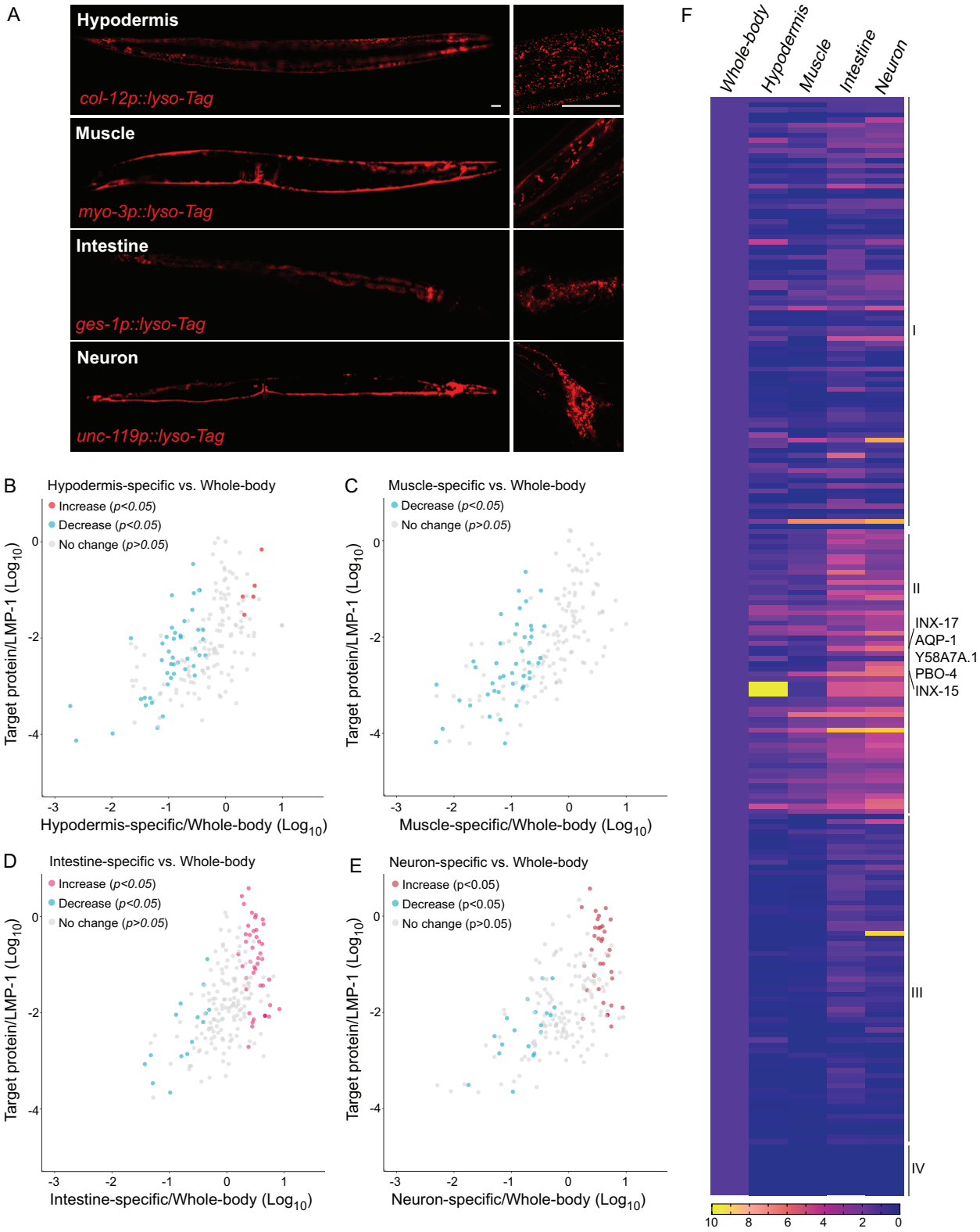

Figure 5. Lysosomal proteome heterogeneity across tissues

1074 **(A)** Example images of transgenic strains carrying Lyso-Tag (LMP-1::RFP-3×HA) driven by
1075 tissue-specific promoters. Scale bar=20 μm.
1076 **(B-E)** Scatter plot showing the relative enrichment ratio for each of 216 lysosome-enriched
1077 proteins identified from whole-body LMP-1 Lyso-IP in comparison with tissue-specific LMP-1
1078 Lyso-IPs, hypodermis (**B**), muscle (**C**), intestine (**D**) and neuron (**E**). X axis, enrichment ratio
1079 tissue-specific vs. whole-body; Y axis, normalized protein abundance over LMP-1; each dot
1080 represents the average of three replicates.
1081 **(F)** Heatmap showing the relative enrichment of 216 lysosome-enriched proteins identified from
1082 whole-body LMP-1 Lyso-IP in comparison with tissue-specific LMP-1 Lyso-IPs. Group I,
1083 comparable ratios between whole-body and tissue-specific Lyso-IPs; Group II, increase in tissue-
1084 specific Lyso-IPs ($p<0.05$ by student's t-test); Group III, decrease in tissue-specific Lyso-IPs
1085 ($p<0.05$ by student's t-test); Group IV, absent in tissue-specific IPs.
1086

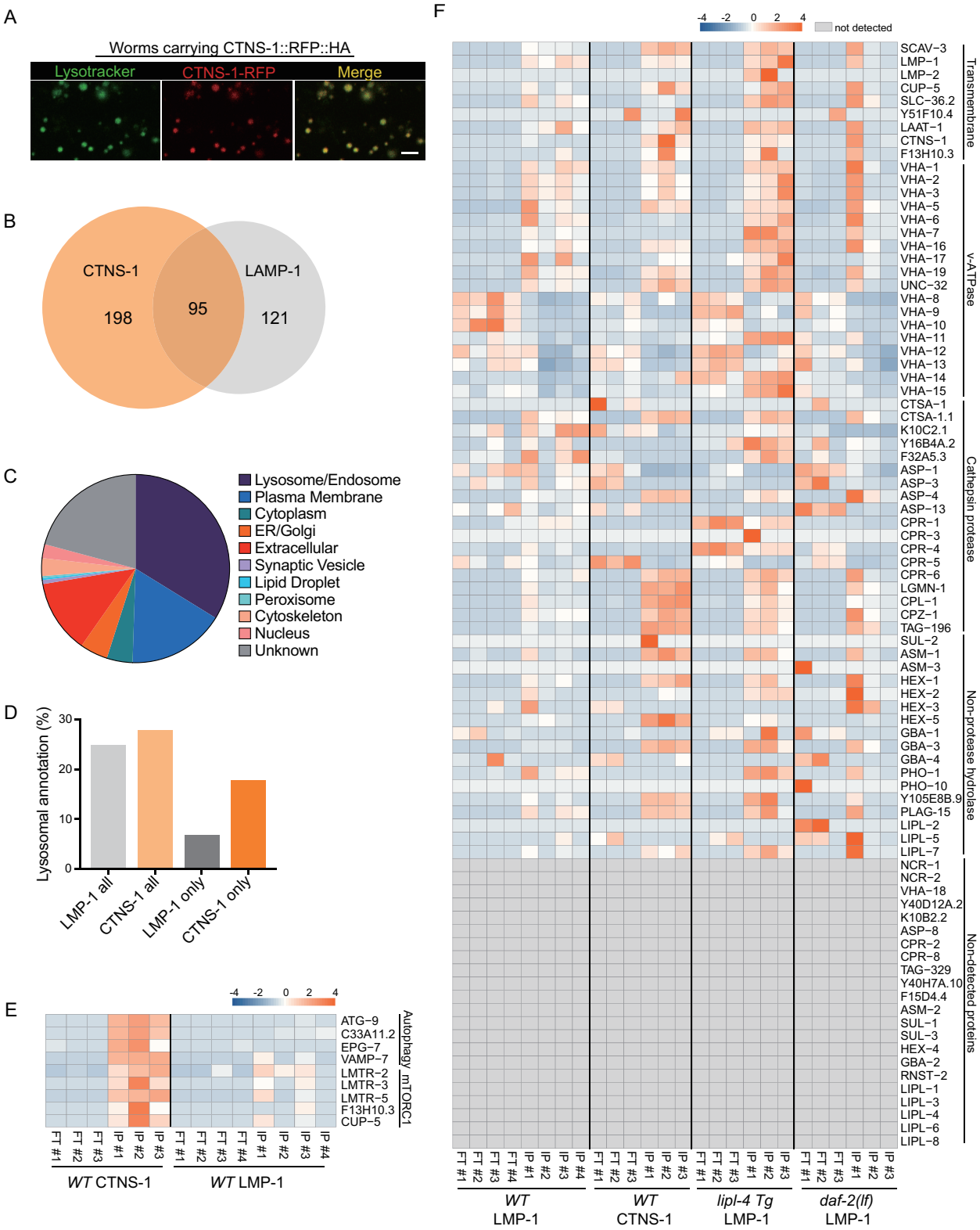

1087

1088 **Figure 6. Lysosome-enriched proteome identified with Cystinosin**

1089 **(A)** Example images of transgenic strains carrying CTNS-1 Lyso-Tag (CTNS-1::RFP-3×HA)
1090 with LysoTracker staining to mark lysosomes *in vivo*. Scale bar=5 μm.
1091 **(B)** Venn diagram showing the overlap between lysosome-enriched proteomes using LMP-1
1092 Lyso-IP and CTNS-1 Lyso-IP.
1093 **(C)** Pie chart showing subcellular location categories of lysosome-enriched proteins.
1094 **(D)** The proportion of candidates with lysosomal localization annotation in different candidate
1095 groups. "LMP-1 all" and "CTNS-1 all", all candidates from LMP-1 Lyso-IP and CTNS-1 Lyso-
1096 IP, respectively; "LMP-1 only" and "CTNS-1 only", candidates only identified from LMP-1
1097 Lyso-IP or CTNS-1 Lyso-IP, respectively.
1098 **(E)** Normalized protein levels (z-score across samples) of autophagy-related components and
1099 mTORC1 signaling factors from LMP-1 and CTNS-1 Lyso-IP proteomic analyses of WT
1100 worms.
1101 **(F)** Normalized protein levels (z-score across samples) of previously annotated lysosomal
1102 proteins from LMP-1 Lyso-IP proteomic analyses of WT, *lipl-4 Tg* and *daf-2(lf)*) worms and
1103 CTNS-1 Lyso-IP proteomic analyses of WT worms. Proteins not detected by proteomic profiling
1104 are marked in grey.
1105

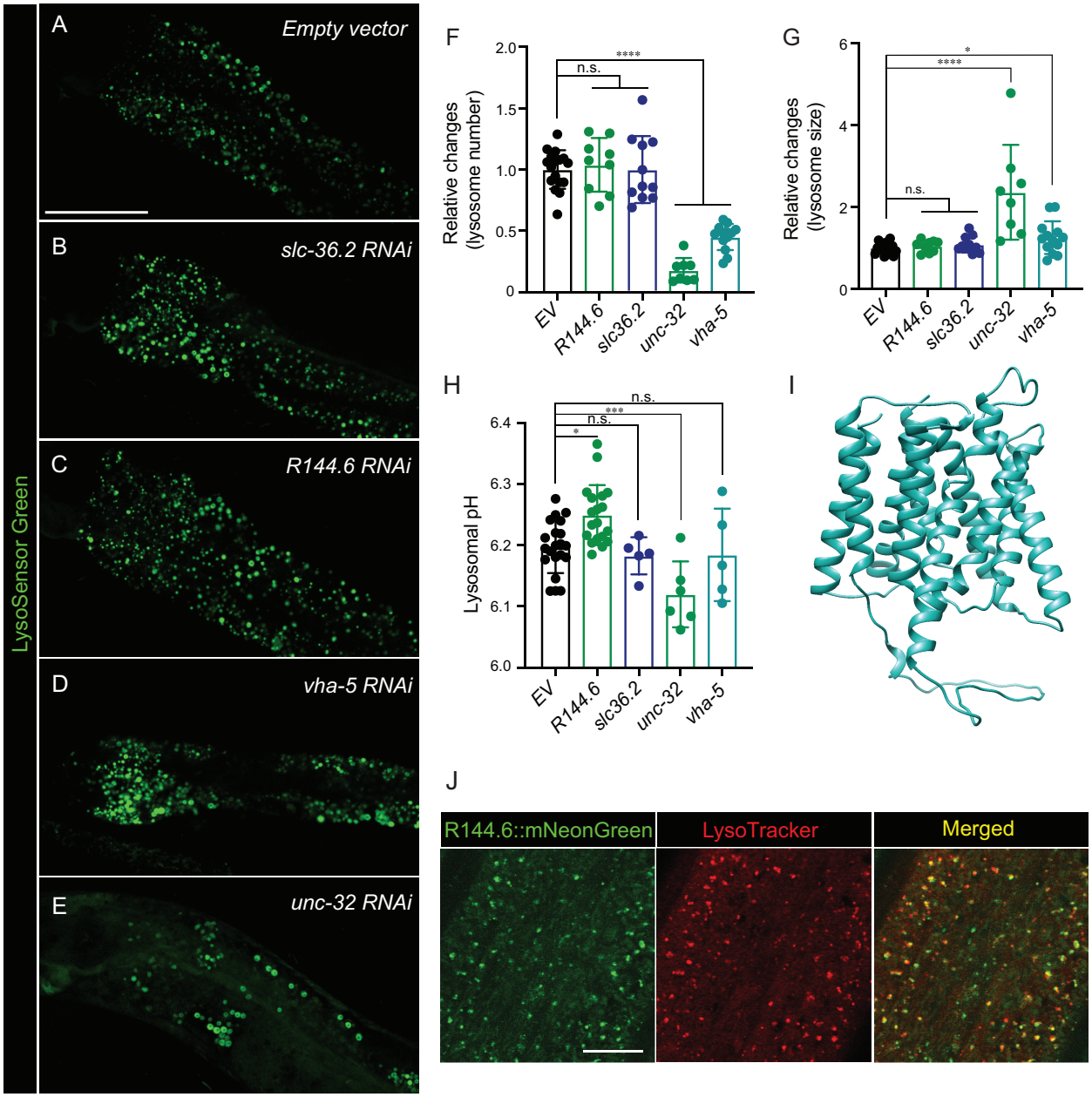

Figure 7. Lysosome-enriched proteins regulating lysosomal functions

(**A-E)** Confocal fluorescence microscopy images of intestinal cells in worms stained with LysoSensor DND-189 and treated with *empty vector* (**A**), *slc36.2* RNAi (**B**), *R144.6* RNAi (**C**), *vha-5* RNAi (**D**) and *unc-32* RNAi (**E**). Scale bar=50 µm.

(F, G) RNAi knockdown of *unc-32* or *vha-5* decreases the lysosome number *(****p< 0.0001)* (**F**) but increases the lysosome size *(****p< 0.0001, *p=0.0222)* (**G**). The average lysosome

1113 number and size per pair of intestinal cells were quantified. Data are shown as mean ± SD.

1114 Student's t-test (unpaired, two-tailed) was performed between the *empty vector* group and each

1115 RNAi-treated group. n = 17(*EV*), 9(*R144.6*), 11(*slc36.2*), 8(*unc-32*), 13(*vha-5*). n.s. *p>0.05,*

1116 (**H**) RNAi knockdown of *R144.6 (*p= 0.0206)* and *unc-32 (***p= 0.0001)* increase and

1117 decrease lysosomal pH, respectively. Lysosomal pH was calculated based on LysoSensor's

1118 lifetime measured by Fluorescence Lifetime Microscopy**.** Data are shown as mean ± SD.

1119 Student's t-test (unpaired, two-tailed) was performed between the *empty vector* group and each

1120 RNAi-treated group. n = 21(*EV*), 19(*R144.6*), 5(*slc36.2*), 6(*unc-32*), 5(*vha-5*). n.s. *p>0.05.*

1121 **(I)** The structure of the R144.6 protein predicted by AlphaFold2 supports it as a solute carrier

1122 family transporter.

1123 **(J)** Confocal fluorescence microscopy images show that mNeonGreen signals from

1124 endogenously tagged R144.6 colocalize with LysoTracker Red signals in the hypodermis. Scale

1125 bar=10 μm.

1126

1127 **SUPPLEMENTARY FIGURES**

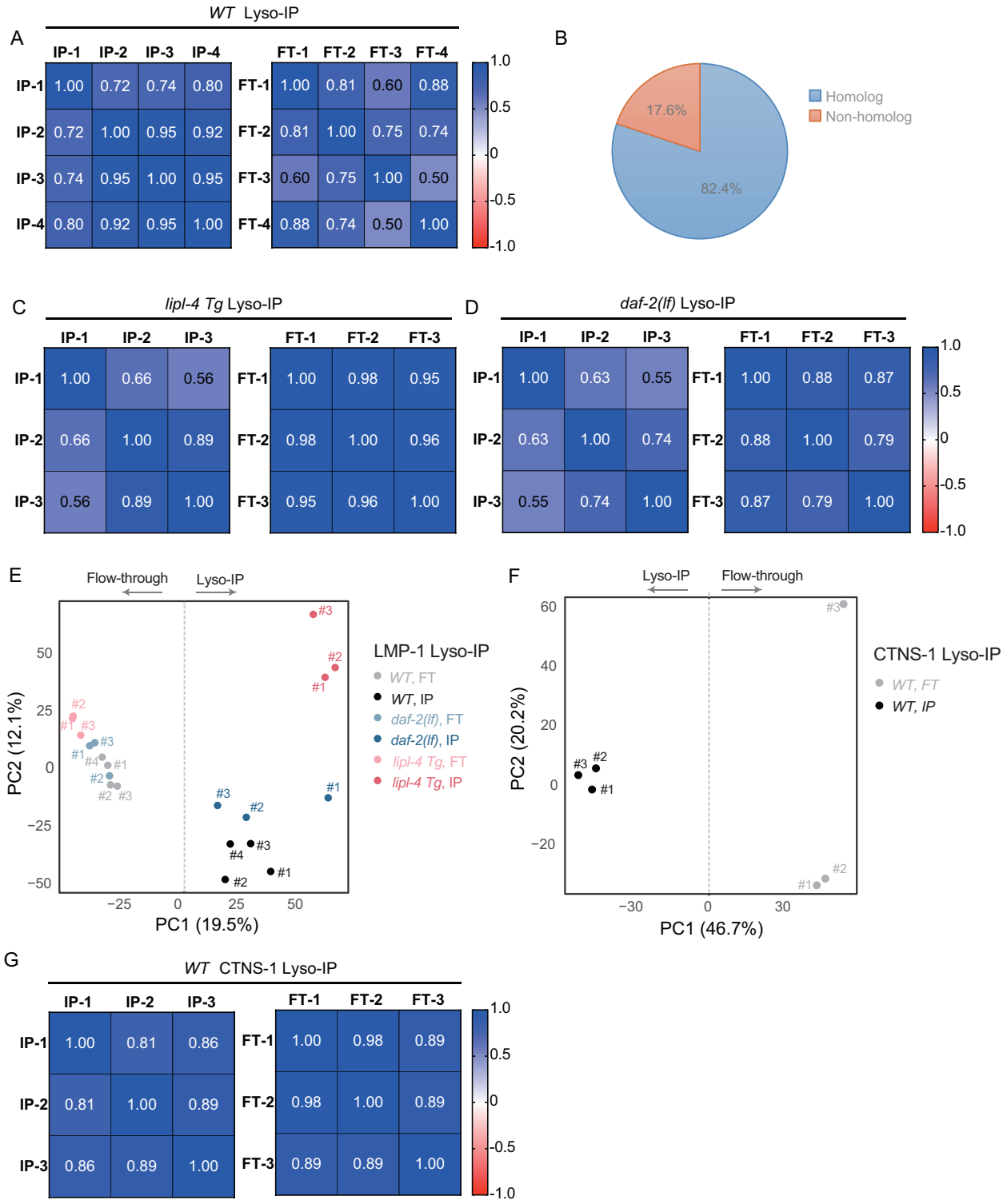

1128

1129 **Supplementary Figure 1. Lyso-IP analyses from worms with different genotypes**

1130 (**A**) Correlation analysis of four independent biological replicates of Lyso-IP (IP) and Flow-
1131 through (FT) samples from proteomics analyses.
1132 **(B)** Pie chart showing the proportion of LMP-1 Lyso-IP candidates from WT worms with
1133 mammalian homologs.
1134 (**C** and **D)** Correlation analysis of three independent biological replicates of Lyso-IP (IP) and
1135 Flow-through (FT) from proteomics analyses of the long-lived *lipl-4* transgenic strain (*lipl-4 Tg*,
1136 **C**) and the *daf-2* loss-of-function mutant (*daf-2(lf)*), **D**).
1137 **(E)** PCA analysis of Lyso-IP replicates and flow-through controls in LMP-1 Lyso-IP of WT,
1138 *lipl-4 Tg* and *daf-2(lf)* worms.
1139 **(F)** PCA analysis of Lyso-IP replicates and flow-through controls of CTNS-1 Lyso-IP of WT
1140 worms.
1141 **(G)** Correlation analysis of three independent biological replicates of Lyso-IP (IP) and Flow-
1142 through (FT) samples from proteomic analyses of CTNS-1 Lyso-IP.
1143

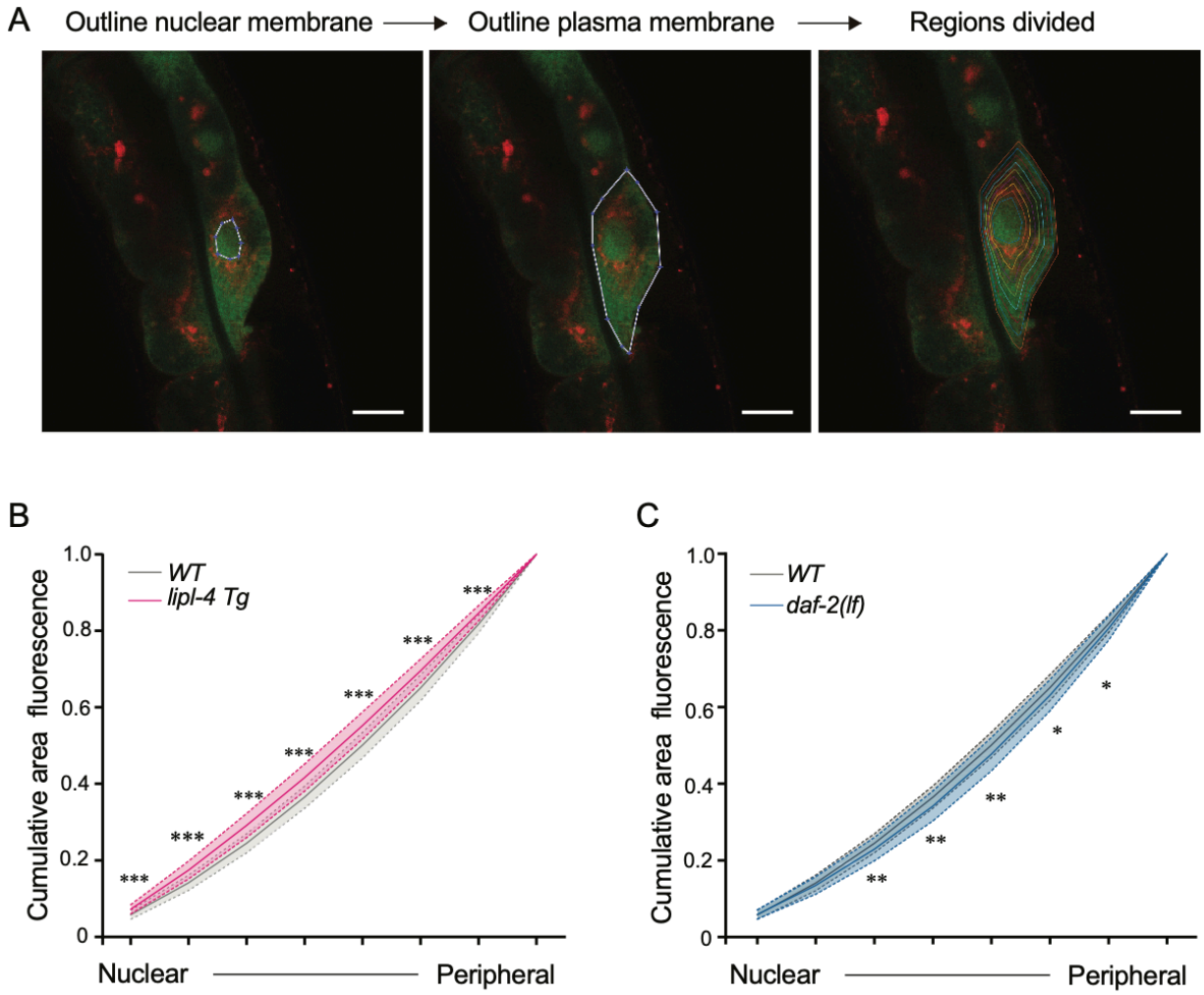

Supplementary Figure 2. Quantitative analysis of lysosomal positioning

(**A**) Brief summary of the method flow for quantifying the lysosomal distribution in intestinal cells of *C. elegans*. Scale bar=10 µm.

(B, C) Curve graph showing the normalized accumulated intensity of lysosomal signals from the nuclear to the peripheral region in WT, *lipl-4 Tg* (**B**) and *daf-2(lf)* (**C**) animals. *$p<0.05$; **$p<0.01$, ***$p<0.001$, ****$p<0.0001$, n.s. $p>0.05$ by Student's t-test (unpaired, two-tailed) for each region. N =50 WT /33 *lipl-4 Tg*, 33 WT/ 28 *daf-2(lf)*. Data are represented as mean ± SD. *p* values for (B) (from left to right): 2.65×10^{-8}, 3.19×10^{-8}, 7.93×10^{-8}, 3.62×10^{-7}, 4.79×10^{-6}, 2.98

1153 x10^{-5}, 4.41 x10^{-5}; *p* values for (C) (from left to right): 0.357, 0.0529, 0.00611, 0.00246, 0.00985,

1154 0.0261, 0.0423.

1155

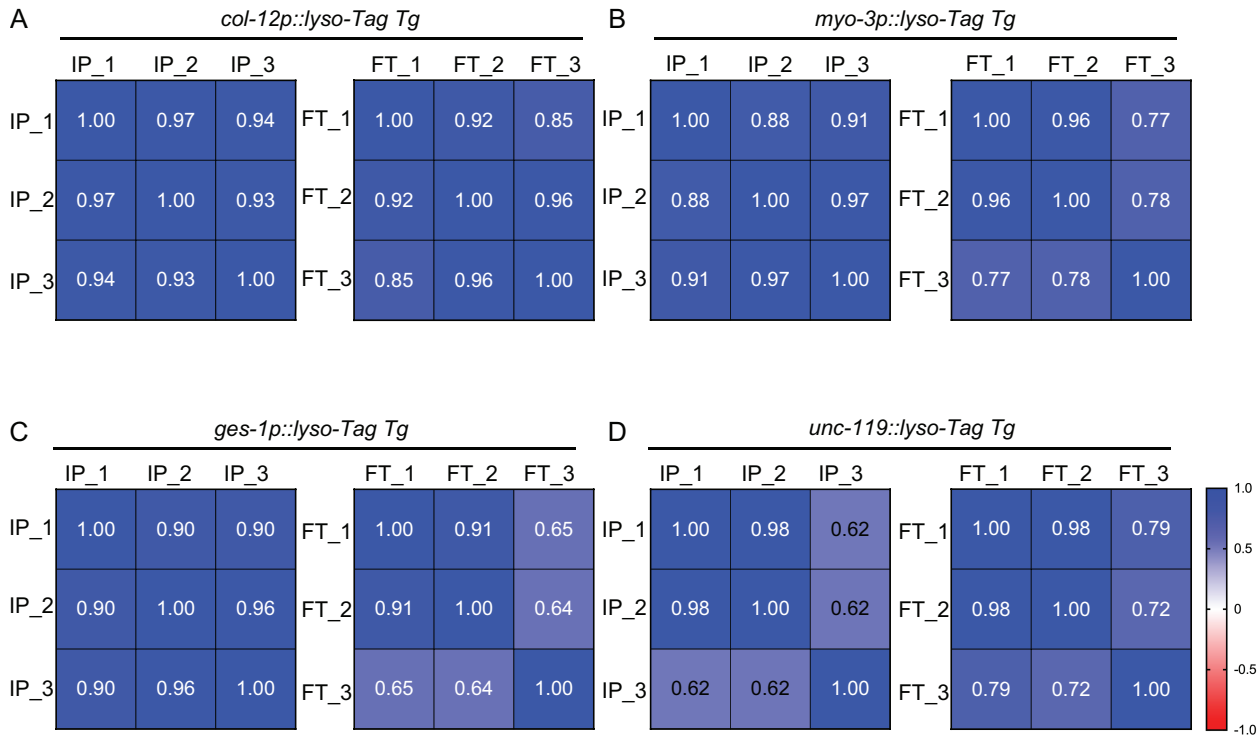

1156

1157 **Supplementary Figure 3. Correlation analyses of tissue-specific Lyso-IPs**

1158 **(A-D)** Pearson Correlation matrices of tissue-specific lyso-IP (IP) samples and flow-through

1159 (FT) samples show the correlation among three different replicates. **(A)** Hypodermis, **(B)**

1160 Muscle, **(C)** Intestine, **(D)** Neuron.

1161

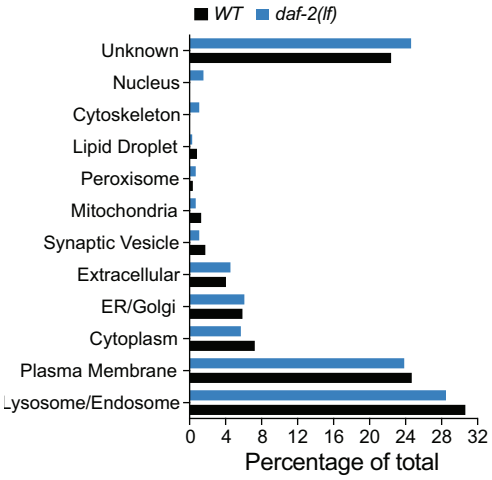

Supplementary Figure 4. Subcellular category analyses of *daf-2(lf)* candidates

The percentage of proteins with different subcellular localization is compared between lysosome-enriched proteomes from WT and *daf-2(lf)* worms.

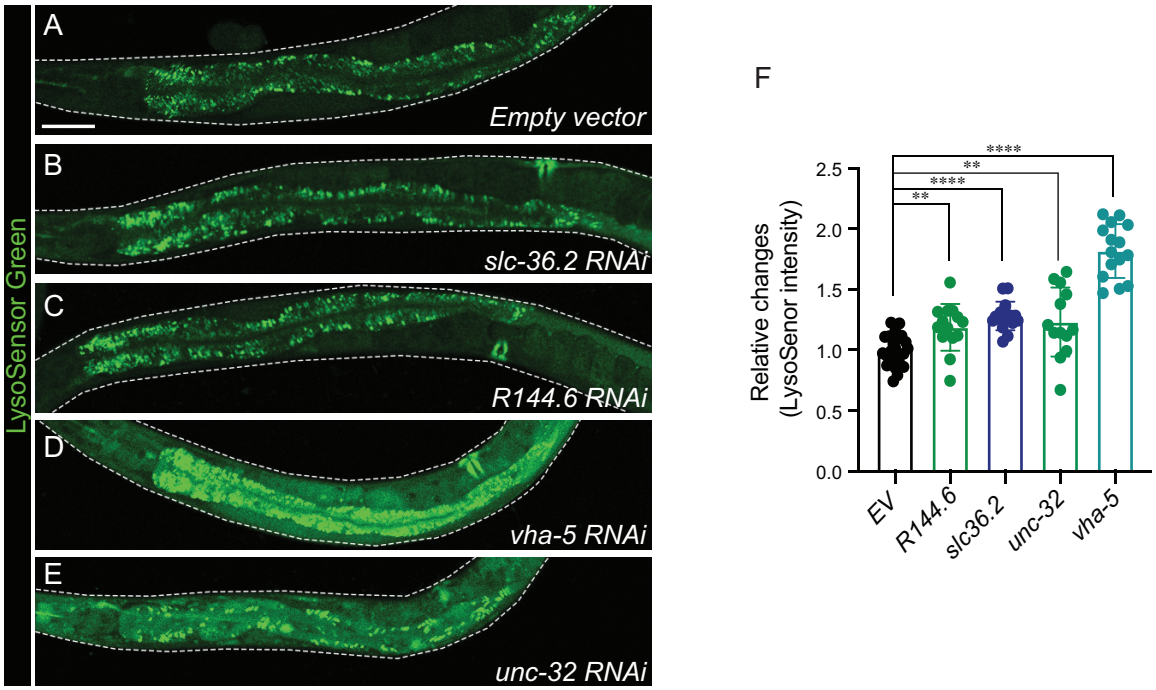

Supplementary Figure 5. Inactivation of lysosome-enriched candidates increases LysoSensor signal intensity

1170 (**A-E)** Confocal fluorescence microscopy images of intestinal cells in worms stained with
1171 LysoSensor DND-189 and treated with *empty vector* (**A**), *slc36.2* RNAi (**B**), *R144.6* RNAi (**C**),
1172 *vha-5* RNAi (**D**) and *unc-32* RNAi (**E**). Scale bar=50 μm.
1173 **(F)** RNAi knockdown of *slc36.2 (****p<0.0001), R144.6 (**p=0.0011), unc-32 (**p=0.0019)*
1174 *or vha-5 (****p<0.0001)* increases the LysoSensor signal intensity in the area of the first pair of
1175 intestinal cells. Data are shown as mean ± SD. Student's t-test (unpaired, two-tailed) was
1176 performed between the *empty vector* group and each RNAi-treated group. n = 24 (*EV*), 14
1177 (*R144.6*), 13 (*slc36.2*), 15 (*unc-32*), 16 (*vha-5*).
1178
1179 **Supplementary Table 1. Lysosome-enriched proteins identified from LMP-1 Lyso-IP using**
1180 **WT worms**
1181 **Supplementary Table 2. Lysosome-enriched proteins identified from LMP-1 Lyso-IP using**
1182 ***lipl-4 Tg* worms**
1183 **Supplementary Table 3. Summary of lifespan analyses**
1184 **Supplementary Table 4. Lysosome-enriched proteins identified from LMP-1 Lyso-IP using**
1185 ***daf-2(lf)* mutant**
1186 **Supplementary Table 5. Lysosome-enriched proteome exhibits tissue-specificity**
1187 **Supplementary Table 6. Lysosome-enriched proteins identified from CTNS-1 Lyso-IP**
1188 **using WT worms**
1189 **Supplementary Table 7. LysoSensor screening of lysosome-enriched proteins shared**
1190 **between LMP-1 and the CTNS-1 Lyso-Ips**
1191 **Supplementary code. Matlab code for lysosome distribution quantification**